

# Hidden Markov Individual-level Models of Infectious Disease Transmission

Dirk Douwes-Schultz<sup>1\*</sup>, Rob Deardon<sup>1,2</sup> and Alexandra M. Schmidt<sup>3</sup>

<sup>1</sup>*Department of Mathematics and Statistics, University of Calgary, Canada*

<sup>2</sup>*Faculty of Veterinary Medicine, University of Calgary, Canada*

<sup>3</sup>*Department of Epidemiology, Biostatistics and Occupational Health,  
McGill University, Canada*

February 17, 2026

## Abstract

Individual-level epidemic models are increasingly being used to help understand the transmission dynamics of various infectious diseases. However, fitting such models to individual-level epidemic data is challenging, as we often only know when an individual's disease status was detected (e.g., when they showed symptoms) and not when they were infected or removed. We propose an autoregressive coupled hidden Markov model to infer unknown infection and removal times, as well as other model parameters, from a single observed detection time for each detected individual. Unlike more traditional data augmentation methods used in epidemic modelling, we do not assume that this detection time corresponds to infection or removal or that infected individuals must at some point be detected. Bayesian coupled hidden Markov models have been used previously for individual-level epidemic data. However, these approaches assumed each individual was continuously tested and that the tests were independent. In practice, individuals are often only tested until their first positive test, and even if they are continuously tested, only the initial detection times may be reported. In addition, multiple tests on the same individual may not be independent. We accommodate these scenarios by assuming that the probability of detecting the disease can depend on past

---

\*Corresponding author: Dirk Douwes-Schultz, Department of Mathematics and Statistics, University of Calgary, 2500 University Drive NW, Calgary, AB, Canada, T2N 1N4. E-mail: [dirk.douwesschultz@ucalgary.ca](mailto:dirk.douwesschultz@ucalgary.ca).

observations, which allows us to fit a much wider range of practical applications. We illustrate the flexibility of our approach by fitting two examples: an experiment on the spread of tomato spot wilt virus in pepper plants and an outbreak of norovirus among nurses in a hospital.

**Key words :** Bayesian inference; Infectious disease modelling; Coupled hidden Markov model; Markov chain Monte Carlo methods; Data augmentation; Stochastic epidemic model.

## 1 Introduction

Epidemiologists are often interested in questions related to the transmission of an infectious disease at the individual level. For example, whether susceptibility differs by individual-level characteristics such as age (Cohen et al., 1997; Davies et al., 2020), or how far an infected individual could realistically spread the disease (Hu et al., 2021; Lichtenberg et al., 2022). Individual-level models (ILMs) of infectious disease transmission (Deardon et al., 2010) can be valuable tools for helping answer these types of questions (Vynnycky and White, 2010). These approaches model each individual in the population moving through different disease states, such as susceptible, infectious, and removed (Ward et al., 2025). Transitions between states can occur in continuous (Almutiry et al., 2021) or discrete (Warriyar et al., 2020) time. We will focus on discrete time. For discrete-time models, the probability of infection at each time step may depend on the number of infectious individuals in the population, their distance from the susceptible individual, and the inherent susceptibility or infectivity of individuals, which may vary with covariates (Keeling et al., 2001; Mahsin et al., 2022). Therefore, these models can describe a wide range of complex mixing patterns.

However, a significant challenge with fitting ILMs to individual-level epidemic data is that we usually only know when an individual was detected (e.g, showed symptoms), not when they were infected or removed (Touloupou et al., 2020). For example, in Section 4.2, we look at an experiment on the spread of tomato spotted wilt virus (TSWV) in pepper plants, which was described in Hughes et al. (1997) and analyzed using ILMs by Almutiry et al. (2021). The experimenters only monitored a plant until symptoms of TSWV appeared, so that the data consists of a single detection time for each detected plant (corresponding to observed symptom onset). Since symptoms of TSWV take 2-4 weeks to appear in a plant, plants were likely infected before they were detected. Furthermore, signs of TSWV can be difficult to spot in a plant; therefore, it is possible that the experimenters never detected some infected plants. In this example, we do not know the infection or removal times or even how many plants were infected, which makes inference challenging.

The most popular way to account for uncertain infection and removal times in epidemic

modelling is to treat them as unknown parameters of the model within a Bayesian framework, which is known as data augmentation (DA) (O'Neill, 2002; O'Neill and Kypraios, 2019). Most DA methods assume that infection times are unknown and removal times are known (O'Neill and Roberts, 1999; Deardon et al., 2010; O'Neill and Kypraios, 2019), or that infection times are known and removal times are unknown (Bu et al., 2022). However, in many applications, we do not observe when individuals were removed or infected (Neal and Roberts, 2004; Pokharel and Deardon, 2022). In such cases, a susceptible-infectious-notified-removed (SINR) model (Jewell et al., 2009) can be used to estimate unknown infection and removal times using observed notification (detection) times (Almutiry et al., 2021). In an SINR model, all infectious individuals must enter the notified state before transitioning to the removed state. That is, these models assume that all infectious individuals must be detected before removal. However, infectious individuals could recover without being detected if, for example, they show mild or no symptoms and testing is based on the appearance of symptoms (Mullis et al., 2009). In addition, studies that use SINR models have made much stronger assumptions. For example, Jewell et al. (2009) assumed that the notification and removal times were known. Almutiry et al. (2021) did not require the removal times to be known. However, they assumed that only those who showed symptoms were infected. It is possible for individuals who did not show symptoms to have been infected, if they had asymptomatic infections, hard to spot symptoms, or were infected late in the study and had not yet developed symptoms (Jewell et al., 2009). The assumption that no undetected individuals were infected during the observation period is common when using many existing DA methods (Britton and O'Neill, 2002). This is because, if there are undetected infections, traditionally complex reversible jump Markov chain Monte Carlo (MCMC) steps must be used to add and remove infection times (O'Neill and Roberts, 1999; Jewell et al., 2009).

Taking a very different approach, Touloupou et al. (2020) proposed using a coupled hidden Markov model (Pohle et al., 2021) to account for unknown infection and removal times for discrete-time ILMs. They first assumed that the epidemiological states of the individuals (e.g., susceptible, infectious, and removed) followed a series of coupled hidden Markov chains. By coupled, we mean that the transition probabilities of an individual chain, like the probability of going from susceptible to infectious, could depend on whether other individuals were in the infectious state. Then they generated the detection times conditional on the hidden states using an independent Bernoulli observation model. There are many important advantages of this approach over the more traditional DA methods described in the previous paragraph. Firstly, unlike most of those methods, their model does not assume that any of the detection times correspond to infection or removal times. In addition, unlike the SINR approach of Almutiry et al. (2021), infectious individuals do not have to be detected

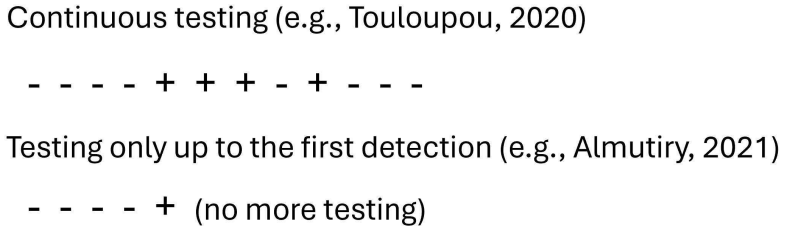


**Figure 1:** Shows the difference between continuous testing, assumed in Touloupou et al. (2020), and testing only up to the first detection, which is more common in epidemiological studies.

before removal, and undetected individuals (e.g., those who did not show symptoms) may have been infected during the study. Finally, all hidden state indicators for an individual can be sampled directly from their full conditional distribution using the individual forward filtering backward sampling (iFFBS) algorithm (Touloupou et al., 2020). This means that there is no need to use complex reversible jump MCMC steps to add or remove infection times.

However, Touloupou et al. (2020) assumed that each individual was continuously tested for the disease (see Figure 1) and that the tests were independent. In epidemiological studies, individuals are often only tested until they are first detected, like in the TSWV example described above, or the time of first detection may be the only available information (Stockdale et al., 2017; Mizumoto and Chowell, 2020; Almutiry et al., 2021). In addition, tests on the same individual may not be independent.

To address the above limitations, we extend the approach of Touloupou et al. (2020) by letting the probability of detecting the disease depend on past observations. This allows us to establish a stopping rule for the testing or reporting based on when an individual is first detected. The resulting hidden Markov model is very general. It only requires a single detection time (e.g., corresponding to symptom onset) for each detected individual. Additionally, it does not assume this detection time corresponds to infection or removal, and does not require infectious individuals to be detected at any point. We also show how more traditional DA methods can be incorporated into our framework, such as those assuming known removal (O'Neill and Roberts, 1999) or infection (Bu et al., 2022) times. This allows these methods to be fit without the use of reversible jump MCMC steps. Also, since we fit all models under a unified approach, comparing them using the widely applicable information criterion (WAIC) (Gelman et al., 2014) is straightforward. This provides a data-driven procedure to help choose between different DA methods (represented by separate observation models), which has not been considered in the literature to the best of our knowledge.

The remainder of this paper is organized as follows. Section 2 introduces the proposed

hidden Markov model for outbreak investigations in which there is only a single detection time for each detected individual. Section 3 discusses our Bayesian inferential procedure, which makes use of the computationally efficient iFFBS algorithm of Touloupou et al. (2020). In Section 4, we fit our proposed model to two examples: an outbreak of norovirus in a hospital and an experiment on the spread of tomato spotted wilt virus in pepper plants. We also compare our approach to several popular alternatives from the literature, such as models that assume known infection or removal times or that no undetected individuals were infected. We close with a discussion in Section 5.

## 2 Hidden Markov Individual Level Modelling Framework

Assume we have a population of  $i = 1, \dots, N$  individuals who are observed across  $t = 1, \dots, T$  time periods. Individual-level epidemic data usually takes the form of a collection of detection times for each individual. Let  $y_{it} = 1$  if individual  $i$  was detected as having the disease during time  $t$  (e.g., showed symptoms), and 0 otherwise. We focus on the case where there is at most a single detection time for each individual; see Section 2.1. This means that, for the detected individuals,  $y_{it}$  will be equal to 0 until their single detection time, then it will be one, and then zero again until the end of the study; see the bottom graph of Figure 2. Finally, let  $S_{it}$  be an indicator for the true epidemiological state of the individual, where

$$S_{it} = \begin{cases} 1, & \text{if individual } i \text{ was susceptible during time } t, \\ 2, & \text{if individual } i \text{ was infectious,} \\ 3, & \text{if individual } i \text{ was removed.} \end{cases}$$

The detection times  $y_{it}$  are observed, while the epidemiological states  $S_{it}$ , which are of primary interest, are latent, unobservable quantities. Therefore, we use a coupled hidden Markov model (Pohle et al., 2021) to infer the parameters of an SIR ILM from the observed detection times. This involves first specifying an observation model that describes how the detection times are generated conditional on the disease states. Then we specify a Markov model describing how the disease states evolve over time.

### 2.1 A general autoregressive observation process

Touloupou et al. (2020) considered a continuous testing observation model, which strongly implies that there should be multiple detection times for at least some of the detected individuals; see Section 4.2. However, it is much more common with individual-level outbreak data to have only a single detection time for each detected individual (e.g., corresponding to

symptom onset) (Stockdale et al., 2017; Kypraios et al., 2017; O’Neill and Kypraios, 2019; Stockdale et al., 2021; Almutiry et al., 2021). If there is only a single detection time per detected individual, then either individuals were only tested until they were first detected (see Figure 1), which is common in epidemiological studies (Mizumoto and Chowell, 2020; Almutiry et al., 2021), or individuals were continuously tested and only the initial detection times were reported by investigators. In this section, we show that both of these scenarios lead to the same observation model.

Firstly, we will assume that individuals are only tested for the disease until they are first detected. For example, in the TSWV experiment analyzed in Section 4.2, plants were only checked for symptoms until they first appeared (Hughes et al., 1997). The tests could be laboratory-based (Touloupou et al., 2020); visual and based on the appearance of symptoms (Almutiry et al., 2021); or some combination of the two (Mizumoto and Chowell, 2020). In general, we view a test as any procedure, such as checking for symptoms, that has a non-zero probability of detecting the disease if it is present. We will also assume that there are no false positives, as otherwise identifiability may be challenging with only one detection time available for each detected individual.

If individuals are only tested until they first test positive, the probability that an infectious individual is detected will be given by the sensitivity of the test,  $\theta > 0$ , until the individual is first detected, and then it will be 0, as the testing stops (if an individual is not tested, they will not be detected). Therefore, we specify the observation model as

$$y_{it} \mid S_{it}, y_{i0}, \dots, y_{i(t-1)} \sim \begin{cases} 0, & \text{if } S_{it} = 1 \text{ or } 3 \text{ (susceptible or removed)} \\ \text{Bern}(\theta \mathbb{I}[y_{i0}, \dots, y_{i(t-1)} = 0]), & \text{if } S_{it} = 2 \text{ (infectious),} \end{cases} \quad (1)$$

where we assume  $y_{i0} = 0$ , that no individuals were detected before the study started. In (1),  $\mathbb{I}[y_{i0}, \dots, y_{i(t-1)} = 0]$  is an indicator function which will be 1 if individual  $i$  was not detected previously and 0 if individual  $i$  was detected previously. Figure 2 shows a diagram of the model for a single detected individual.

If there is only a single detection time for each detected individual, it could also be that individuals were continuously tested, but only the initial detection times were reported. For example, outbreak investigations often only report the symptom onset time for each detected individual (Thompson and Foege, 1968; Cáceres et al., 1998). If the decision to report a test only depends on whether the individual was previously detected, then (1) is still an appropriate observation model. To see this, we can first shift perspective from the investigators to the modeler (or any outside observer) and assume  $y_{it}$  represents whether the modeler detects the disease in an individual. Then the probability that the modeler detects

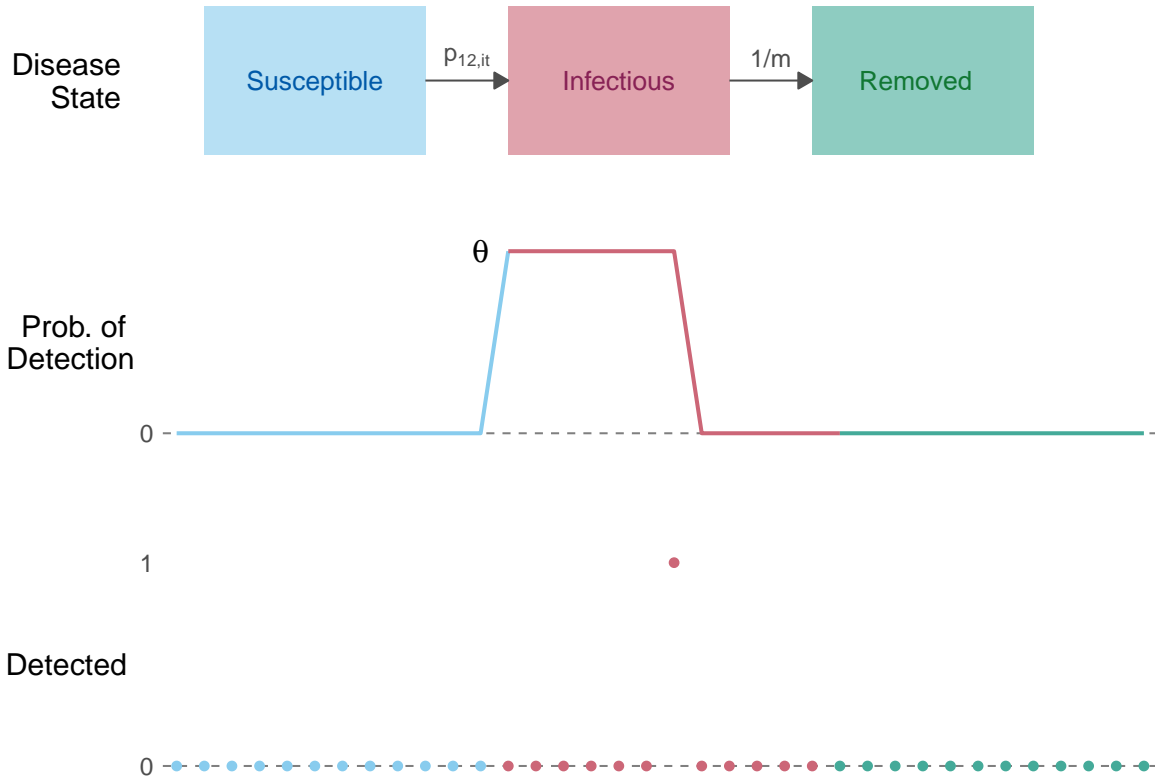


**Figure 2:** Shows a diagram of the proposed hidden Markov individual-level model (HMM-ILM) for a single hypothetical detected individual. The bottom graph shows the observations  $y_{it}$ .

the disease will be  $\theta$  until the individual is first detected, and then it will be 0, since if a test is not reported, the modeler will not detect the disease.

Finally, we note that the testing does not necessarily have to be independent over time as in Touloupou et al. (2020). For example, suppose that the test results of infectious individuals follow a first-order Markov chain, so that the probability of testing positive is  $\theta$  if the individual previously tested negative and  $\theta_1$  if the individual previously tested positive, with  $\theta_1 > \theta$ . Since individuals are only tested until they first test positive, all test results up to the detection time are negative, which means (1) still holds.

## 2.2 The hidden underlying SIR ILM

We assume that the disease state of individual  $i$ ,  $S_{it}$ , follows a three-state nonhomogeneous Markov chain. In order to account for disease spread between individuals, we condition the transition matrix on  $\mathbf{S}_{(-i)(t-1)} = (S_{1(t-1)}, \dots, S_{(i-1)(t-1)}, S_{(i+1)(t-1)}, \dots, S_{N(t-1)})^T$ , the vector of disease states for all individuals excluding individual  $i$  at time  $t-1$ . We propose the

following conditional transition matrix for the Markov chain, for  $t = 1, \dots, T$ ,

$$\Gamma(S_{it} | \mathbf{S}_{(-i)(t-1)}) = \begin{array}{c|ccc} \text{State} & S_{it}=1 \text{ (sus.)} & S_{it}=2 \text{ (inf.)} & S_{it}=3 \text{ (rem.)} \\ \hline S_{i(t-1)}=1 \text{ (sus.)} & 1 - p_{12,it} & p_{12,it} & 0 \\ S_{i(t-1)}=2 \text{ (inf.)} & 0 & 1 - \frac{1}{m} & \frac{1}{m} \\ S_{i(t-1)}=3 \text{ (rem.)} & 0 & 0 & 1 \end{array}, \quad (2)$$

where  $\Gamma(S_{it} | \mathbf{S}_{(-i)(t-1)})_{lk} = P(S_{it} = k | S_{i(t-1)} = l, \mathbf{S}_{(-i)(t-1)})$  and  $m$  is the average duration of the infectious period, which we will discuss more below.

In (2),  $p_{12,it}$  represents the probability that individual  $i$  is infected in the interval  $[t-1, t)$  if they are susceptible at time  $t-1$ . We will assume individual  $i$  primarily makes contacts within a neighborhood  $NE(i)$ . Let  $\beta_{j \rightarrow i,t}$  be the probability of an infectious contact between individuals  $i$  and  $j \in NE(i)$  in the interval  $[t-1, t)$ . Also, suppose there is a small constant risk  $\alpha$  of an individual being infected by someone outside their neighborhood (potentially outside the population) or a background reservoir. Then, assuming all contacts are independent, we have

$$\begin{aligned} p_{12,it} &= 1 - (1 - \alpha) \prod_{j \in NE(i)} (1 - \beta_{j \rightarrow i,t})^{I[S_{j(t-1)}=2]} \\ &\approx 1 - \exp \left( -\alpha - \sum_{j \in NE(i)} \beta_{j \rightarrow i,t} I[S_{j(t-1)}=2] \right), \end{aligned} \quad (3)$$

which follows the classic Reed-Frost formulation of a discrete-time SIR model (Vynnycky and White, 2010; Deardon et al., 2010). Note that the approximation (3) holds only when  $\beta_{j \rightarrow i,t}$  is small for all  $j \in NE(i)$ , which may not be appropriate if some individuals in the population are closely connected. Therefore, we more generally interpret  $\beta_{j \rightarrow i,t} > 0$  as the effect of disease spread from individual  $j$  to individual  $i$  in the continuous time interval  $[t-1, t)$ , and we generally do not restrict it to be less than 1.

Deardon et al. (2010) proposed a very flexible form for the effects of disease spread,  $\beta_{j \rightarrow i,t} = \mathcal{S}_i \mathcal{T}_j \mathcal{K}_{ij}$ , where  $\mathcal{S}_i > 0$  is a susceptibility function for susceptible individual  $i$ ,  $\mathcal{T}_j > 0$  is a transmissibility function for infective  $j$ , and  $\mathcal{K}_{ij} > 0$  is an infection kernel representing some contact measure between  $i$  and  $j$  (e.g., distance). This form has been extended in a myriad of ways, for example, to allow for geographically varying parameters (Mahsin et al., 2022) and to account for covariate measurement error (Amiri et al., 2024). For ease of exposition, and since we mainly focus on the observation model, we assume a more generic

specification for the effect of disease spread between individuals,

$$\beta_{j \rightarrow i, t} = g(\boldsymbol{\beta}, \mathbf{x}_{ijt}), \quad (4)$$

where  $g(\cdot)$  is a positive-valued function,  $\boldsymbol{\beta}$  is a vector of unknown parameters, and  $\mathbf{x}_{ijt}$  is a vector of covariates. For example,  $\mathbf{x}_{ijt}$  could include the distance between individuals  $i$  and  $j$  (Almutiry et al., 2021), the age of individual  $i$  or  $j$  (Becker, 1989), or a temporal indicator for the implementation of some control measure (Lekone and Finkenstädt, 2006).

In (2),  $m > 1$  represents the average duration of the infectious period. The advantage of specifying the probability of removal as  $1/m$  is that there is usually good prior information available for  $m$  (Lappe et al., 2023). However, we must be cautious in interpreting  $m$  for some applications, as individuals can be removed from the population before they naturally recover from the disease; see Section 4.1. Finally, we need to specify an initial state distribution for the Markov chain, that is,  $P(S_{i0} = k)$  for  $i = 1, \dots, N$  and  $k = 1(\text{susceptible}), 2(\text{infectious}), 3(\text{removed})$ . This should be done based on knowledge of the outbreak, for example, based on who was likely the index case; see Section 4.1. For our examples, we will assume  $P(S_{i0} = 3) = 0$ .

We will call the model defined by Equations (1)-(4) the hidden Markov individual-level model (HMM-ILM). Note that the HMM-ILM, unlike most other epidemic models that employ DA methods (O'Neill and Kypraios, 2019), does not assume that the detection times correspond to either infection or removal times (see Figure 2). Additionally, from (1), infectious individuals can go undetected if they never test positive. This means the HMM-ILM can account for infections with mild or no symptoms, when the testing is based on the appearance of symptoms, or infections that occur near the end of the study and are not yet showing symptoms. That is, the HMM-ILM allows for both  $S \rightarrow I \rightarrow R$  and  $S \rightarrow I$  transitions among undetected individuals. This is in contrast to the popular existing DA methods described in the introduction (O'Neill and Roberts, 1999; Almutiry et al., 2021), which, recall, do not allow for  $S \rightarrow I \rightarrow R$  transitions among undetected individuals. Furthermore, while  $S \rightarrow I$  transitions among undetected individuals (e.g., infections that occur near the end of the study) can be incorporated into traditional DA methods, complex reversible jump MCMC steps must then be used to add or remove infection times (Jewell et al., 2009). Therefore, many approaches assume no undetected individuals were infected (O'Neill and Kypraios, 2019; Almutiry et al., 2021), meaning they cannot account for late or asymptomatic infections. As we show in the next section, another advantage of the HMM-ILM is a unified Bayesian inferential procedure where the hidden disease states for an individual are sampled directly from their full conditional distribution (Touloupou et al.,

2020); no complex reversible jump MCMC steps or Metropolis-Hastings proposals for the states are required.

### 3 Inferential Procedure

We will first show that the HMM-ILM is a hidden Markov model. Let  $\mathbf{S}_t = (S_{1t}, \dots, S_{Nt})^T$  be the vector of epidemiological state indicators for all individuals at time  $t$ ,  $\mathbf{y}_t = (y_{1t}, \dots, y_{Nt})^T$  be the vector of observations for all individuals at time  $t$ ,  $\mathbf{S} = (\mathbf{S}_0, \dots, \mathbf{S}_T)^T$ , and  $\mathbf{y} = (\mathbf{y}_1, \dots, \mathbf{y}_T)^T$ . The vector  $\mathbf{S}_t$  follows a first-order nonhomogeneous Markov chain with state space  $\{1, 2, 3\}^N$  and  $3^N$  by  $3^N$  transition matrix  $\Gamma(\mathbf{S}_t)$ . From Equation (2), an element of  $\Gamma(\mathbf{S}_t)$  is given by,

$$P(\mathbf{S}_t = \mathbf{s}_t | \mathbf{S}_{t-1} = \mathbf{s}_{t-1}) = \prod_{i=1}^N P(S_{it} = s_{it} | S_{i(t-1)} = s_{i(t-1)}, \mathbf{S}_{(-i)(t-1)} = \mathbf{s}_{(-i)(t-1)}),$$

where  $\mathbf{s}_t, \mathbf{s}_{t-1} \in \{1, 2, 3\}^N$ . Therefore, rewriting the HMM-ILM model in terms of  $\Gamma(\mathbf{S}_t)$  and  $p(\mathbf{y}_t | \mathbf{y}_0, \dots, \mathbf{y}_{t-1}, \mathbf{S}_t) = \prod_{i=1}^N p(y_{it} | y_{i0}, \dots, y_{i(t-1)}, S_{it})$ , for  $t = 1, \dots, T$ , and  $p(\mathbf{S}_0) = \prod_{i=1}^N p(S_{i0})$  shows that it is a hidden Markov model (see Chapter 10 of Frühwirth-Schnatter (2006)). However, the size of the transition matrix ( $3^N$  by  $3^N$ , where  $N$  is usually at least around 100) necessitates some changes to the standard inferential procedure of such models (Frühwirth-Schnatter, 2006), as we will now discuss.

Let  $\mathbf{v} = (\theta, m, \alpha, \boldsymbol{\beta})^T$  denote the vector of all model parameters. The joint distribution of  $\mathbf{y}$  and  $\mathbf{S}$  given  $\mathbf{v}$  is given by

$$p(\mathbf{y}, \mathbf{S} | \mathbf{v}) = \prod_{i=1}^N p(S_{i0}) \prod_{t=1}^T p(S_{it} | S_{i(t-1)}, \mathbf{S}_{(-i)(t-1)}, m, \alpha, \boldsymbol{\beta}) p(y_{it} | y_{i0}, \dots, y_{i(t-1)}, S_{it}, \theta). \quad (5)$$

For the detected individuals, we only observe the disease state indicator  $S_{it}$  when they are detected, that is, only at the single point where  $y_{it} = 1$  (then we must have  $S_{it} = 2$  as we assume no false positives). For the undetected individuals, we never observe  $S_{it}$ . It is also not possible to marginalize  $\mathbf{S}$  from (5) to calculate  $L(\mathbf{v}) = p(\mathbf{y} | \mathbf{v})$ , the marginal likelihood function, as doing so would require matrix multiplication with  $\Gamma(\mathbf{S}_t)$  (Frühwirth-Schnatter, 2006). Therefore, we treat the disease state indicators as unknown parameters of the model and sample  $\mathbf{S}$  and  $\mathbf{v}$  from their joint posterior distribution, which is proportional to

$$p(\mathbf{S}, \mathbf{v} | \mathbf{y}) \propto p(\mathbf{y}, \mathbf{S} | \mathbf{v}) p(\mathbf{v}), \quad (6)$$

where  $p(\mathbf{v})$  is the prior distribution of  $\mathbf{v}$ . Often, good prior information is available for  $m$  (the

average duration of infectiousness) and/or  $\theta$  (the probability of initial detection). However, we must be cautious when interpreting these parameters for a given application, as discussed in more detail in the examples in Section 4. Regardless of the prior specification, the joint posterior distribution is not available in closed form. Therefore, we used a hybrid Gibbs sampling algorithm with some steps of the slice sampling or Metropolis-Hastings algorithms to sample from it. We sampled  $m$  and  $\theta$  using either univariate slice samplers (Neal, 2003) or adaptive random walk Metropolis steps (Shaby and Wells, 2010), depending on the mixing. Since  $(\alpha, \beta)^T$  showed high posterior correlations, we jointly sampled it using automated factor slice sampling (Tibbits et al., 2014).

It is straightforward to sample the state indicators one at a time from their full conditional distributions,  $p(S_{it}|\mathbf{S} \setminus \{S_{it}\}, \mathbf{y}, \mathbf{v})$  (Douwes-Schultz and Schmidt, 2022). However, we found that this mixed so slowly in our two examples and simulation studies that it is not usable. Jointly sampling all of  $\mathbf{S}$  from  $p(\mathbf{S}|\mathbf{y}, \mathbf{v})$  usually results in much faster mixing when fitting HMMs (Chib, 1996). However, this is not possible with the HMM-ILM, as it again requires matrix multiplication with  $\Gamma(\mathbf{S}_t)$ . Therefore, we instead jointly sampled each individual's disease state indicators, conditional on the disease state indicators for all other individuals, using the individual forward filtering backward sampling (iFFBS) algorithm (Touloupou et al., 2020). More specifically, the iFFBS algorithm samples the vector of all state indicators for individual  $i$ ,  $\mathbf{S}_{i(0:T)} = (S_{i0}, \dots, S_{iT})^T$ , from its full conditional distribution,

$$p(\mathbf{S}_{i(0:T)}|\mathbf{S}_{(-i)(0:T)}, \mathbf{y}, \mathbf{v}) = p(S_{iT}|\mathbf{S}_{(-i)(0:T)}, \mathbf{y}, \mathbf{v}) \prod_{t=0}^{T-1} p(S_{it}|S_{i(t+1)}, \mathbf{S}_{(-i)(0:t+1)}, \mathbf{y}_{i(0:t)}, \mathbf{v}), \quad (7)$$

where  $\mathbf{S}_{(-i)(0:T)}$  is  $\mathbf{S}$  with  $\mathbf{S}_{i(0:T)}$  removed; see Supplemental Materials (SM) Section 1 for additional details.

The hybrid Gibbs sampling algorithm was implemented using the R package NIMBLE (de Valpine et al., 2017). NIMBLE comes with built-in slice and automated factor slice samplers. We implemented the iFFBS samplers using NIMBLE's custom sampler feature. All NIMBLE R code and data for our motivating examples are available on GitHub [https://github.com/Dirk-Douwes-Schultz/HMM\\_ILM\\_Code](https://github.com/Dirk-Douwes-Schultz/HMM_ILM_Code). In SM Section 2, we present a simulation study that shows our proposed Gibbs sampler can recover the true parameter values of an HMM-ILM, which is specified like in our TSWV example in Section 4.2.

Finally, we note that to run the iFFBS algorithm, we only require  $S_{it}|\mathbf{S}_{(-i)(t-1)}$  to follow a first-order Markov chain and for  $y_{it}$  to depend only on  $S_{it}$  and, potentially, on past observations (see Section 2.2.1 of Douwes-Schultz (2024) for a list of exact conditions). Therefore, it is very easy to modify the HMM-ILM. For example, in Section 4.1, for comparison purposes,

we modify the observation process (1) so that individuals are removed as soon as they are detected (O'Neill and Roberts, 1999). Currently in the literature, even very similar ILMs are often fit with vastly different MCMC algorithms (Jewell et al., 2009; Almutiry et al., 2021). A more unified inferential procedure, as we present here, could make these models more easily adoptable for practitioners.

## 4 Applications

To fit all models discussed in this section, we ran our hybrid Gibbs sampling algorithm for 200,000 iterations on three chains with an initial burn-in of 50,000 iterations. All chains were started from random values in the parameter space to avoid convergence to local modes. Convergence was checked using the Gelman–Rubin statistic (all estimated parameters  $< 1.05$ ), the minimum effective sample size ( $> 1000$ ), and by visually examining the traceplots (Plummer et al., 2006). Unless indicated otherwise, no convergence issues were apparent for any model discussed in this section.

### 4.1 Norovirus outbreak in a South Carolina hospital

For our first example, we analyze a norovirus outbreak among 89 nurses in a South Carolina hospital in January 1996 (Cáceres et al., 1998). The observation period for the outbreak investigation extended from the 5th to the 13th ( $t=1, \dots, T=9$ ). The data consists of 28 detection times, one for each detected nurse, which correspond to the day the nurse first reported showing symptoms in a survey administered by investigators. Figure 3 shows the epidemic curve, that is, the number of new cases over time. The first case was Nurse X on the fifth. Nurse X was thought to be the nurse who introduced the infection into the ward, as many of the early cases were traced back to her. The ward was closed on the 12th, and after that, no new cases were reported.

Kypraios et al. (2017) previously analyzed this data using a homogeneously mixing SIR model. However, they assumed that all the removal times in the interval  $[1, T]$  had been observed and were equal to the detection (i.e., symptom onset) times, which is a common assumption following the influential work of O'Neill and Roberts (1999). That is, they assumed that Nurse X was removed on the fifth, that the four nurses detected on the seventh were removed that day, and so on. However, a snowstorm on the seventh forced the nurses to stay overnight at the hospital, so they could not have been removed that day. Also, according to the investigation report (Cáceres et al., 1998), many nurses continued to work after developing symptoms due to staff shortages. Additionally, since Kypraios et al. (2017) assumed they had observed all removal times in the interval  $[1, T]$ , they implicitly assumed

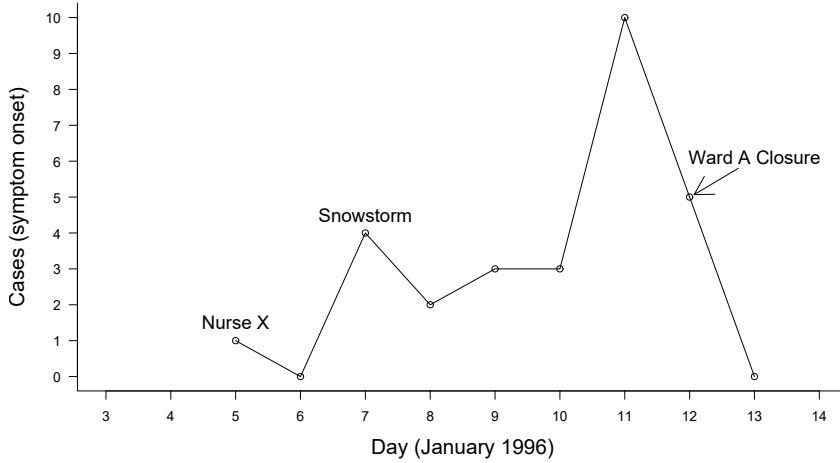


**Figure 3:** Cases in nurses by day of symptom onset. Norovirus outbreak in a South Carolina hospital.

none of the 61 undetected nurses had been removed during the observation period. This is an often overlooked issue with the framework of O’Neill and Roberts (1999). Norovirus can frequently have mild or no symptoms (Wang et al., 2023), meaning it is not unreasonable to assume that at least some of the nurses were infected and recovered without being detected.

In contrast, the HMM-ILM allows individuals to be removed even several days after detection, as illustrated in Figure 2. Additionally, the HMM-ILM allows for  $S \rightarrow I \rightarrow R$  transitions among undetected individuals. Therefore, it may be more suitable for this data. As we have no individual-level information, we used a simple homogeneous mixing model to describe the effects of disease spread between the nurses,

$$\beta_{j \rightarrow i, t} = \beta(1 - W_{t-1}), \quad (8)$$

where  $W_t$  is an indicator for whether the ward was closed that day. That is, we are assuming that if the ward is closed, the nurses will not mix with each other. Given that there is no obvious neighborhood structure, we let  $NE(i) = \{j : j \neq i\}$ . During the outbreak investigation, the nurses were given surveys in which they had to record the day they first showed symptoms. Therefore, we can interpret  $\theta$ , from Equation (1), as the daily probability that an infectious nurse first develops symptoms, multiplied by the probability that the nurse notices (or remembers) symptoms given that they have developed. Finally, for the initial state distributions, we assumed that Nurse X had a 95% chance of being initially infected, as they likely introduced the infection into the ward (Cáceres et al., 1998). We assumed that all other nurses had a low 1% chance of being initially infected.

We first tried to fit the HMM-ILM specified above using wide priors for all parameters. However, with only 28 detection times, the posteriors were very uninformative and the model had trouble converging. Therefore, we decided to use contact tracing information from the outbreak investigation (Cáceres et al., 1998) to specify informative priors for  $\theta$  and  $m > 1$  (the average length of the infectious period). We placed a Beta(40, 40(6/4)) prior on  $\theta$  to reflect an average of 1-2 days from exposure to the first reported appearance of symptoms, which was found by contact tracing. For  $m$ , an individual should be infectious with norovirus for an average of 12 days without any intervention (Lappe et al., 2023). However, it is unlikely that infectious nurses would have worked at the hospital for this entire duration. For example, the investigation report talks about a nurse who first showed symptoms on the seventh, stayed overnight due to the snowstorm, worked the next day, and was not removed until the ninth. Therefore, we assume  $m$  is likely somewhere between 1.5 (average time to first reported symptoms) and 12 days, and we placed a Gamma(2, 2/5.75) prior on  $m - 1$ . Finally, we placed wide Unif(0, 1) priors on  $\beta$  and  $\alpha$ , from Equations (3) and (8).

Figure 4 shows the prior and posterior distributions of  $\theta$ ,  $m$ ,  $\alpha$ , and  $\beta$ . The prior and posterior distributions of  $m$  and, especially,  $\theta$  are very similar, indicating that there is not a lot of information about these parameters in the data. In contrast, the data is much more informative about  $\alpha$  and  $\beta$ . From the posteriors, we estimate that there was a daily background infection risk of 1.4% (0.08%, 4.8%) (posterior median and 95% credible interval), and that the probability of an infectious contact between a susceptible and infectious nurse was 0.65% (0.2%, 1.5%) per day. This implies that an infectious nurse would produce an average of 2.61 (1, 7.04) secondary infections before recovering in a completely susceptible population, which is known as the basic reproduction number  $R_0 = (N - 1)\beta m$  (Vynnycky and White, 2010). The background infection risk could be attributed to the 10 patients who were infected on the ward during the observation period and are not typically included in the model (Britton and O'Neill, 2002; Kypraios et al., 2017). It may also represent infections that are not well explained by the assumptions of the model, such as homogeneous mixing.

We can estimate the number of undetected nurses removed during the observation period by looking at the posterior median and 95% credible interval of  $\sum_{i=29}^{89} I[S_{iT} = 3]$ , which is 9 (1, 31) (we let nurses 29-89 be the undetected ones). Therefore, it is likely that at least a few nurses were infected and recovered without being detected, possibly because they showed no symptoms or did not complete the form accurately. This casts some doubt on the assumption made by Kypraios et al. (2017) that none of the undetected nurses were removed. However, the credible interval, while not including 0, is still very wide with only 28 detection times. Finally, we can better understand how the outbreak evolved over time by examining the posterior probability that a nurse was in each epidemiological state during each day. We

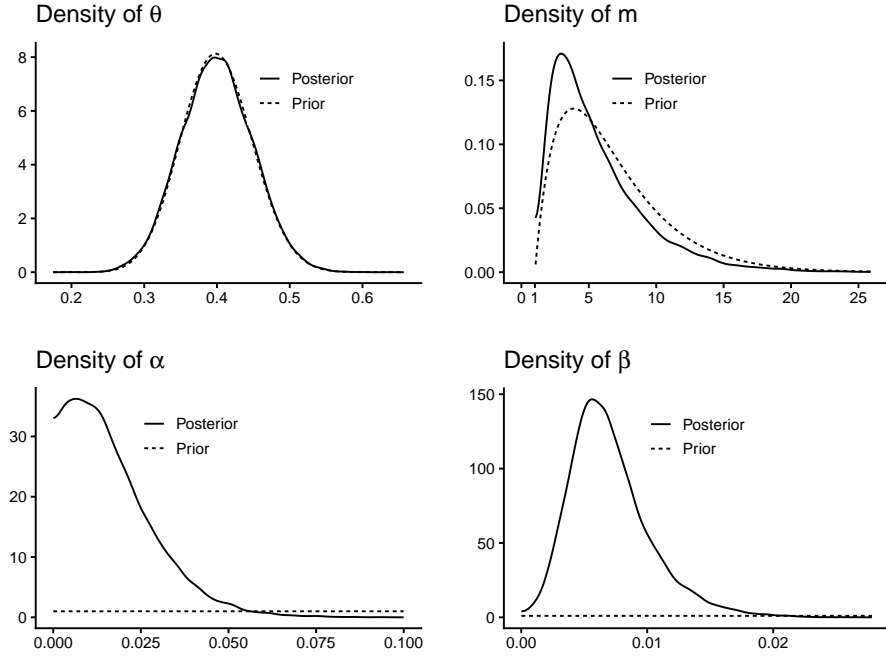


**Figure 4:** Posterior and prior distributions of  $\theta$ ,  $m$ ,  $\alpha$ , and  $\beta$  from fitting the HMM-ILM to the norovirus outbreak data.

do this for one of the 4 nurses detected on the seventh in SM Figure 5. From the figure, this nurse was likely infected on the fifth or sixth and not removed until at least the ninth or tenth, which corresponds to the description of one of the nurses detected on the seventh given in the investigation report (as discussed above). This again casts some doubt on the assumption made in Kypraios et al. (2017) that this nurse was removed on the seventh and would not have been able to infect anyone else on subsequent days. Examining plots of the other nurses showed a similar pattern of at least 2-4 days between detection and removal.

We can incorporate known removal times by modifying the observation process (1),

$$y_{it} \mid S_{it}, y_{i0}, \dots, y_{i(t-1)} \sim \begin{cases} 0, & \text{if } S_{it} = 1 \text{ or } 2 \text{ (susceptible or infectious)} \\ \text{Bern}(\text{I}[y_{i0}, \dots, y_{i(t-1)} = 0]), & \text{if } S_{it} = 3 \text{ (removed).} \end{cases} \quad (9)$$

Note (9) assumes we have observed the removal time of every nurse removed in the interval  $[1, T]$ , and that the removal times are equal to the detection (i.e, symptom onset) times, as in Kypraios et al. (2017) and O'Neill and Roberts (1999) (see above for an indepth discussion of these assumptions). Figure 5 compares the posterior distribution of  $R_0$  between the HMM-ILM described in the previous paragraphs and an HMM-ILM where (1) is replaced by (9), which we will refer to as the known removal times (KRT) model. Assuming known removal

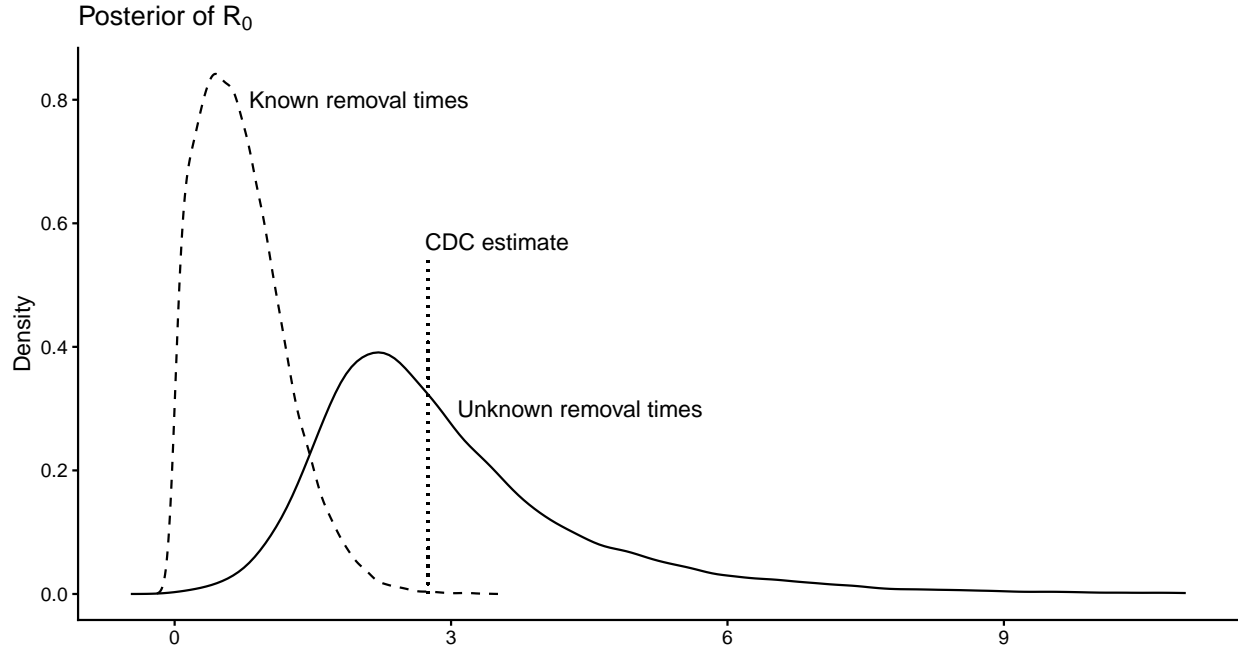


**Figure 5:** Shows the posterior distribution of  $R_0$  for a model that assumes unknown removal times, our HMM-ILM, and a model that assumes known removal times, that is, that the removal times are equal to the detection (i.e., symptom onset) times as in Kypraios et al. (2017). The vertical dotted line is drawn at the median  $R_0$  estimate from Steele et al. (2020).

times, a nurse’s removal time is equal to their reported symptom onset time, meaning we can interpret  $m$  as the average duration from exposure to reported symptoms. Therefore, we placed a  $\text{Unif}(1, 3)$  prior on  $m$  for the KRT model based on the contact tracing discussed above. We kept the other model specifications the same.

From Figure 5, assuming known removal times results in a much smaller and more concentrated posterior for  $R_0$ . A CDC study of 7,094 norovirus outbreaks found a median  $R_0$  estimate of 2.75 (interquartile range 2.38-3.65) (Steele et al., 2020), which is not well represented by the posterior from the KRT model. The posterior median and 95% credible interval of the intercept  $\alpha$  was 3.28% (0.53%, 6.64%) for the KRT model, while, recall, it was 1.4% (0.08%, 4.8%) for our HMM-ILM. A large intercept like this may indicate model misspecification, since it implies that many of the infections cannot be explained by mixing between the nurses. The KRT model attributes a significant portion of the infection risk to background reservoirs, while producing an unrealistically low estimate of the risk from between-nurse mixing, as represented by  $R_0$ .

The two models can also be compared using the widely applicable information criterion (WAIC) (Gelman et al., 2014; Douwes-Schultz et al., 2025), see SM Section 3. The model with the smallest WAIC is considered to have the best fit, and as a rule of thumb, a difference

of 5 or more in the WAIC is considered significant (Reich and Ghosh, 2019). The HMM-ILM had a WAIC of 221, while the KRT model had a WAIC of 222.36. Since the difference in WAIC is less than 5, this comparison is inconclusive. In SM Section 4.2, we carry out a sensitivity analysis in which we fit several alternative models, including those without an intercept or assuming the outbreak had ceased, and we were still unable to find any significant differences in the WAIC. This suggests that the sample size of only 28 detection times may be too small to distinguish between different epidemic models using model comparison criteria. This is despite the fact that important model results can be very sensitive to assumptions about the observation process, as shown in Figure 5. Therefore, caution should be exercised when analyzing smaller outbreaks. If we cannot compare models using comparison criteria, we have to rely more heavily on our a priori assumptions about the outbreak, which can have a large impact on the results. For this example, even though the WAIC is inconclusive, we would argue our HMM-ILM more closely matches the description of the outbreak given in Cáceres et al. (1998) compared with the KRT model, and it also produces more realistic estimates, as discussed above. Note that small sample sizes are common when fitting ILMs to incomplete epidemic data (O'Neill and Roberts, 1999; Britton and O'Neill, 2002; Stockdale et al., 2017, 2021) (all with 40 or fewer detection times).

As we show in the next example, when the sample size is larger, 327 detection times, we often do obtain significant differences in the WAIC. This is true even for models that have similar specifications (like a linear versus a non-linear distance kernel). Additionally, we can use much wider priors for the model parameters and still obtain informative posteriors. Therefore, this example needs to be viewed in the context of its small sample size.

## 4.2 Experiment on the spread of tomato spotted wilt virus in pepper plants

For our second example, we analyze an experiment on the spread of tomato spotted wilt virus (TSWV) in pepper plants, which was described in Hughes et al. (1997). In this experiment, they had  $N = 520$  pepper plants planted in 26 rows of 20 plants each. Plants were checked for symptoms of TSWV every 2 weeks for 14 weeks ( $t = 1, \dots, T = 7$ ). The experimenters stopped monitoring a plant after it first showed symptoms, so that the data consist of a single detection time for each detected plant (corresponding to observed symptom onset). The detection times are plotted on a spatial grid in Figure 6. It is not clear how or where the infection was introduced in the experiment. The first plant was detected at time  $t = 2$ , and 327/520 plants had been detected by the end of the observation period.

Many previous attempts to analyze this data have assumed that the infection times are known and equal to the detection times (Pokharel and Deardon, 2014, 2016; Warriyar et al., 2020; Bilodeau et al., 2024). However, it takes 2-4 weeks for symptoms of TSWV to appear

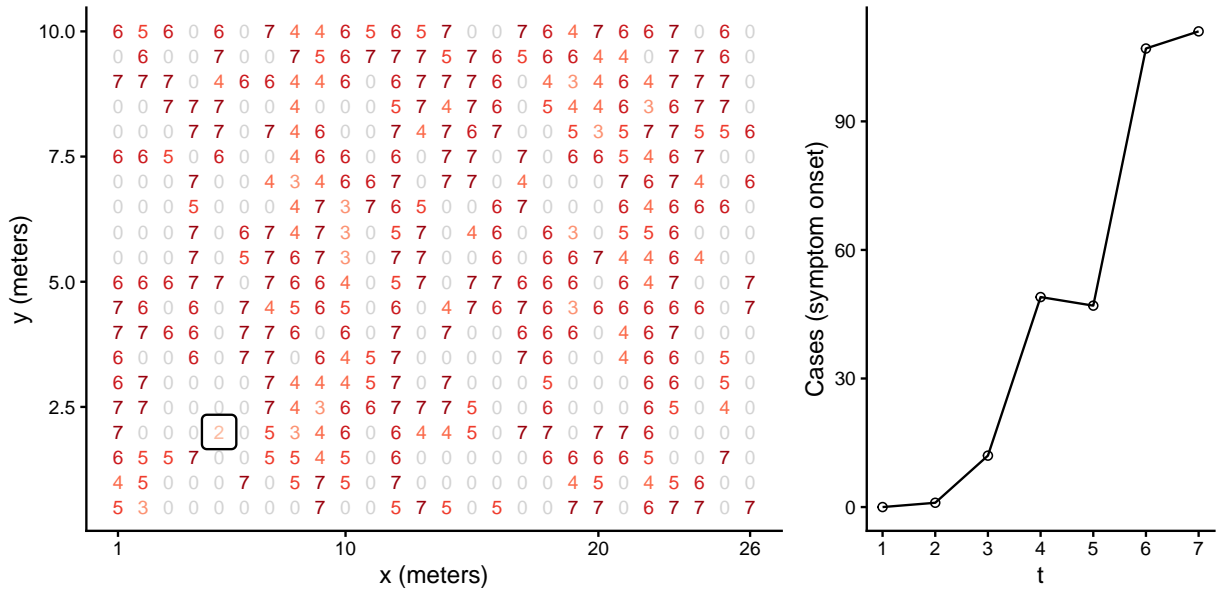


**Figure 6:** The left plot shows the detection time of each detected plant from the experiment in Hughes et al. (1997). A box is drawn around the first plant detected at time  $t = 2$ . A 0 corresponds to the plant never being detected. The right plot shows the epidemic curve.

in a plant (Brust, 2024), meaning plants were likely infected before they were detected. Almutiry et al. (2021) analyzed this data using an SINR model (see the introduction) and estimated the unknown infection and removal times of all 327 detected plants. However, to avoid the use of computationally intensive reversal jump MCMC steps (Jewell et al., 2009), they assumed that none of the 193 undetected plants were infected. Some of the undetected plants could have been infected near the end of the experiment and would have perhaps shown symptoms if the observation period had been extended (it takes 2-4 weeks for symptoms to develop). Indeed, the epidemic curve, plotted in Figure 6, is at its peak, indicating that we would likely see more cases if the experiment had gone on longer. Also, some undetected plants could have had asymptomatic infections or symptoms that were hard to spot (Mullis et al., 2009).

In contrast, the HMM-ILM allows plants to be detected after they have been infected; see Figure 2. Furthermore, the HMM-ILM allows for the possibility that undetected plants were infected and never showed symptoms during the observation period; see Equation (1). Therefore, an HMM-ILM may be more suitable for this data. TSWV is transmitted from plant to plant by small insects called thrips (Mullis et al., 2009). It seems reasonable to assume that the thrips are more likely to move to closer plants compared to those farther away. Therefore, we used a second-order Taylor series approximation of the power-law distance kernel (Deardon et al., 2010) to describe the effect of disease spread between plants

(see Equation (3)),

$$\begin{aligned}\beta_{j \rightarrow i, t} &= \beta_{j \rightarrow i} = \beta_0 \beta_1^{-d_{ij}} \\ &\approx \beta_0 d_{ij}^{-a} (1 - \ln(d_{ij})(\beta_1 - a) + .5 \ln(d_{ij})^2(\beta_1 - a)^2),\end{aligned}\tag{10}$$

where  $d_{ij}$  is the distance (in meters) between plants  $i$  and  $j$ . In (10),  $\beta_0 > 0$  represents the effect of disease spread from plants one meter away, while  $\beta_1 > 0$  represents how fast the effect of disease spread decays with the distance between the two plants. We used a Taylor series approximation as it allows us to factor  $\beta_0$  and  $\beta_1$  from the sums  $\sum_{j \in NE(i)} \beta_{j \rightarrow i, t} I[S_{j(t-1)} = 2]$  in Equation (3). This means we do not need to update these sums when updating  $\beta_0$  and  $\beta_1$  in our MCMC algorithm, which saves a lot of computational time. Note that the Taylor series approximation is always positive. We set  $a = 1.35$ , which is a guess for  $\beta_1$ , from Warriyar et al. (2020). In SM Section 5.1, we investigate some alternative distance kernels, including linear kernels,  $\beta_{j \rightarrow i} = \beta_0 + \beta_1 d_{ij}$ ; quadratic kernels,  $\beta_{j \rightarrow i} = \beta_0 + \beta_1 d_{ij} + \beta_2 d_{ij}^2$  (with positivity constraints); and spline-based kernels. We found the HMM-ILM with Equation (10) had the lowest WAIC by a significant amount, so we use this expansion throughout this section. We also compared the Taylor approximation with the exact power-law and found they had the same WAIC, meaning the Taylor series approximation does not appear to negatively affect the fit.

In this example, we can interpret  $\theta$  as the probability that symptoms develop in a plant multiplied by the probability that the experimenters notice symptoms given that they have developed. Since it is unclear how easy it was to observe the symptoms—they can be hard to spot (Mullis et al., 2009)—we used a wide prior for  $\theta \sim \text{Unif}(0, 1)$ . We also used a wide prior for  $m \sim \text{Unif}(1, 20)$ ,  $\alpha \sim \text{Unif}(0, 1)$ ,  $\beta_0 \sim \text{Unif}(0, 1)$ , and  $\beta_1 \sim \text{Unif}(0, 20)$ . As it is not known how the disease was introduced in the experiment, we assumed each plant had a low 1% chance of being initially infected. Finally, concerning the neighborhood set  $NE(i)$ , there is likely a maximum distance we would expect the thrips to be able to travel within 2 weeks. Therefore, we started with a second-order queen neighborhood structure (all plants at most 2 plants away, including on the diagonal) (Nguyen et al., 2025) and increased the neighborhood order by one until the WAIC decreased by less than 5. The second-order neighborhood model had a WAIC of 1602.68, the third-order model had a WAIC of 1591.76, and the fourth-order model had a WAIC of 1587.32. Therefore, we let  $NE(i)$  include all plants at most three plants away from plant  $i$  (see SM Figure 7).

The top graphs of Figure 7 show the prior and posterior distributions of  $\theta$  and  $m$ . The posterior median and 95% credible interval of  $\theta$  is 0.53 (0.43, 0.65), meaning we estimate that it took an infected plant 1.77 (1.08, 2.65) weeks to be detected on average. This corresponds

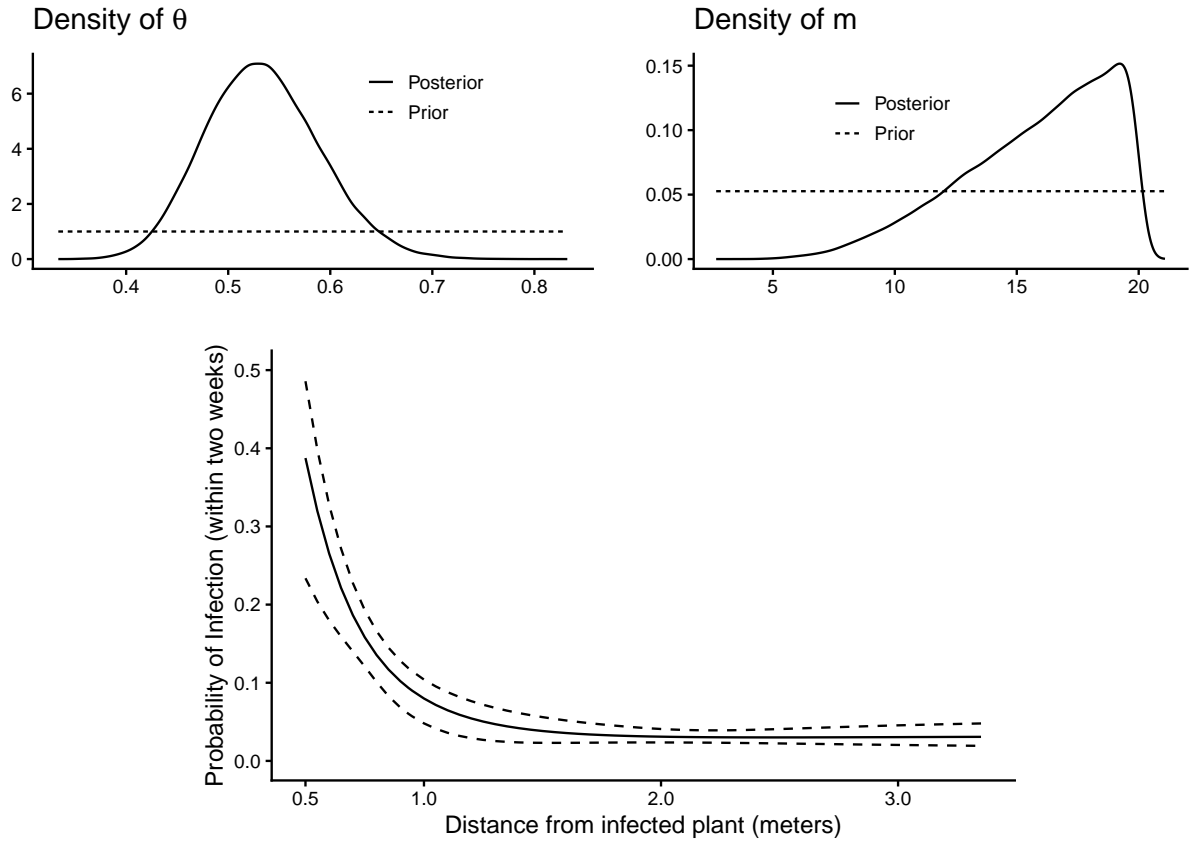


**Figure 7:** The top graphs show the posterior and prior distributions of  $\theta$  and  $m$  from fitting our HMM-ILM to the TSWV experiment. The bottom graph shows the probability that a susceptible plant is infected (within two weeks), given a single infectious plant as a function of the distance between the two plants (posterior median and 95% credible interval).

with the known incubation period (Brust, 2024). Although the posterior of  $m$  is wide, there is a 95% chance that the average duration of the infectious period is at least 20 weeks. Plants are infected with TSWV until they die (Cooper and Meadows, 2024), so a long infectious period like this seems plausible. In our simulation study in SM Section 2, we found that when the true value of  $m$  is greater than  $T$ , the posterior is often wide as seen in Figure 7. In contrast, when the true value of  $m$  is less than  $T$ , the posterior is usually much more concentrated around the true value. This suggests that when the average duration of the infectious period is greater than the length of the observation period, it can be challenging to estimate  $m$ .

The bottom graph of Figure 7 shows the probability that a susceptible plant is infected (within two weeks), given a single infectious plant versus the distance between the two plants. For example, if a susceptible plant is half a meter from an infectious plant (the minimum distance in the experiment), it would have a 39% (23%, 49%) chance of being infected within

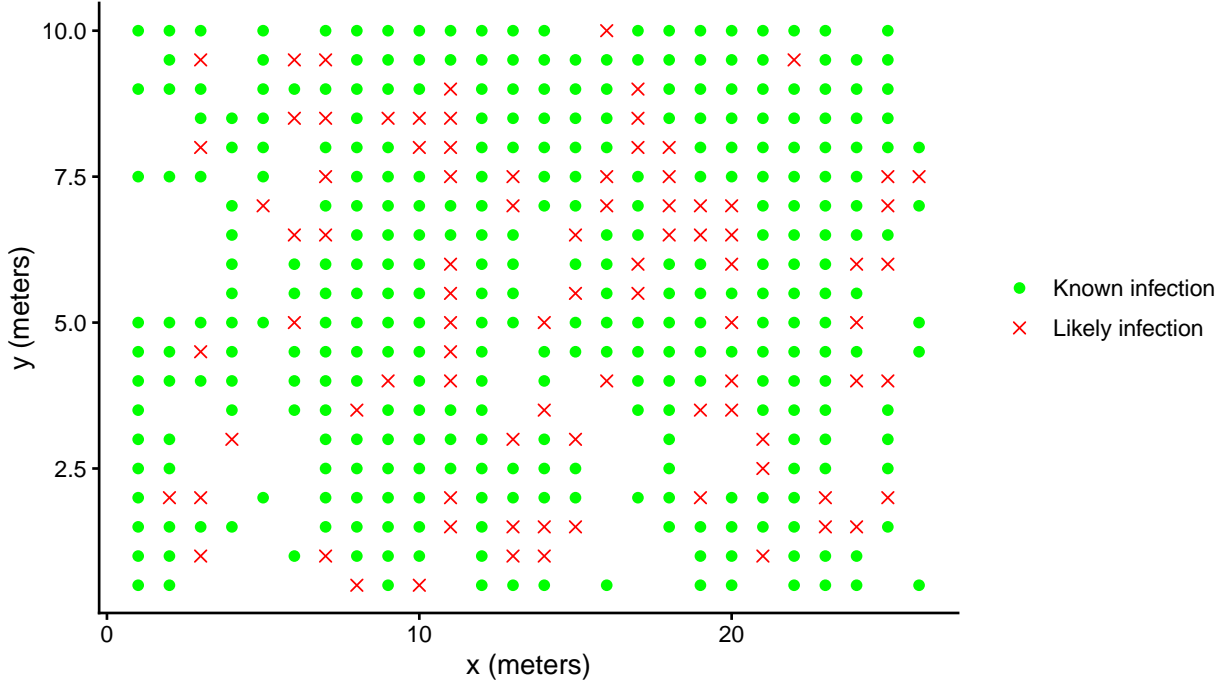


**Figure 8:** The circles represent plants that were detected during the experiment. The crosses represent undetected plants whose posterior probability of having been infected during the experiment,  $P(S_{iT} = 2 \text{ or } 3 \& S_{i0} = 1 | \mathbf{y})$ , is greater than .5.

two weeks. If the plant were 2 meters away, it would have only a 3% (2%, 4%) chance of being infected. Therefore, we can see from the figure that the probability of infection decays very rapidly with the distance from an infected plant. In particular, susceptible plants more than 1.5 meters away from an infected plant are unlikely to be infected within 2 weeks, so the range of dispersal is fairly short. Note that the exact equation plotted, from Equations (3)+(10), is  $1 - \exp(-\alpha - \beta_0 d_{ij}^{-a} (1 - \ln(d_{ij})(\beta_1 - a) + .5 \ln(d_{ij})^2(\beta_1 - a)^2))$  versus  $d_{ij}$ .

The posterior probability that an undetected plant  $i$  was infected during the experiment is given by  $P(S_{iT} = 2 \text{ or } 3 \& S_{i0} = 1 | \mathbf{y}) \approx \frac{1}{Q-M} \sum_{q=M+1}^Q I[S_{iT}^{[q]} = 2 \text{ or } 3 \& S_{i0}^{[q]} = 1]$ , where the superscript  $[q]$  denotes a draw from the posterior distribution of the variable,  $Q$  is the total number of MCMC samples, and  $M$  is the size of the burn-in sample (we removed infections occurring before the experiment ( $t=0$ ) to make things easier to interpret, but the following results are the same either way). Therefore, we can identify undetected plants that were likely infected during the experiment by finding undetected plants  $i$  for which  $P(S_{iT} = 2 \text{ or } 3 \& S_{i0} = 1 | \mathbf{y}) > 0.5$ . We plot the location of such plants in Figure 8 (denoted by crosses). From the figure, we can see that many undetected plants in close proximity to plants that showed symptoms were likely infected during the experiment. These undetected

plants may have had asymptomatic infections or were infected late in the experiment and not yet showing symptoms. We can estimate the total number of undetected plants infected during the experiment by looking at the posterior median and mean of  $\sum_{i: y_{it}=0 \forall t} I[S_{iT} = 2 \text{ or } 3 \& S_{i0} = 1]$ . We find this to be 94 (58, 133). Therefore, even on the low end of our estimation, we would expect 58 of the undetected plants to have been infected during the experiment. This suggests that the analysis from Almutiry et al. (2021), who assumed that none of the undetected plants were infected, was based on over-simplified assumptions.

For comparison purposes, we can incorporate the assumption that no undetected plants were infected, as in Almutiry et al. (2021), by fixing  $S_{it} = 1$  (susceptible) for all undetected plants  $i$  and  $t = 0, \dots, 7$  (see the beginning of the section for an in-depth discussion of this assumption). In this case, we only run the iFFBS algorithm for the 327 detected plants, as the rest of the state indicators are known. We can incorporate known infection times, like in Bilodeau et al. (2024) or Warriyar et al. (2020), by modifying the observation process (1),

$$y_{it} \mid S_{it}, y_{i0}, \dots, y_{i(t-1)} \sim \begin{cases} 0, & \text{if } S_{it} = 1 \text{ or } 3 \text{ (susceptible or removed)} \\ \text{Bern}(I[y_{i0}, \dots, y_{i(t-1)} = 0]), & \text{if } S_{it} = 2 \text{ (infectious).} \end{cases} \quad (11)$$

Note Equation (11) assumes we have observed the infection time of every plant infected in the interval  $[1, T]$ , and that the infection times are equal to the detection times (i.e., when the plant first showed symptoms). This is equivalent to assuming  $\theta = 1$  in Equation (1), that is, that the disease was perfectly detected. Finally, we also want to consider the continuous testing model of Touloupou et al. (2020), since it could be naively applied in an application like this (where we have only a single detection time for each detected individual). Touloupou et al. (2020) assumed individuals kept being tested for the disease even after they were first detected, so that we can replace (1) by,

$$y_{it} \mid S_{it} \sim \begin{cases} 0, & \text{if } S_{it} = 1 \text{ or } 3 \text{ (susceptible or removed)} \\ \text{Bern}(\theta), & \text{if } S_{it} = 2 \text{ (infectious).} \end{cases} \quad (12)$$

Note that if individuals were continuously tested, we would expect to see multiple detection times for at least some of the detected individuals. Having only a single detection time for each detected individual would be very unlikely under this model.

Figure 9 compares the probability of infection versus distance and WAIC of (a) the proposed HMM-ILM, (b) an HMM-ILM with (1) replaced by (12) (Touloupou et al., 2020), (c) an HMM-ILM with (1) replaced by (11) (known infection times), and (d) an HMM-ILM fixing  $S_{it} = 1$  for all undetected plants (no undetected plants infected). For the comparison

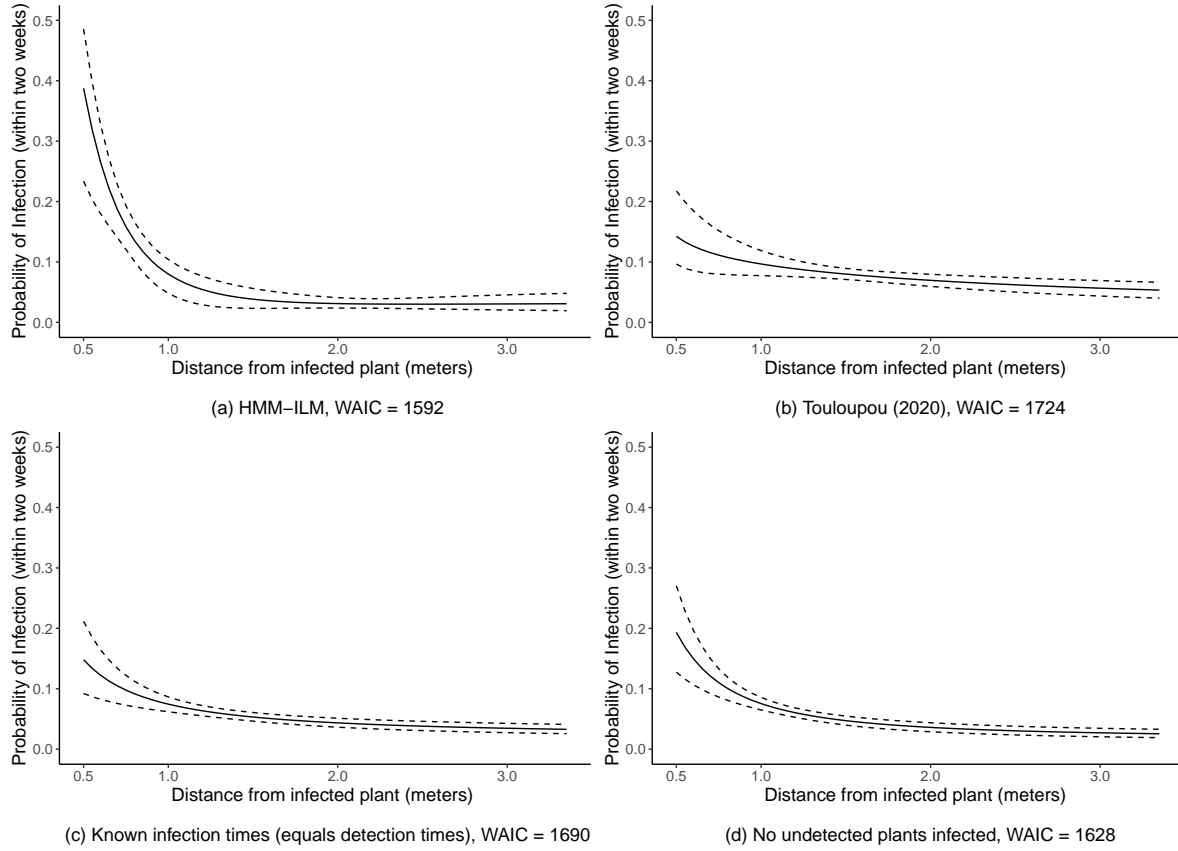


**Figure 9:** Shows the probability that a susceptible plant is infected (within two weeks) given a single infectious plant as a function of the distance between the two plants, for four models fitted to the TSWV experiment. Shows posterior medians and 95% credible intervals.

models, we used the same priors and also kept the other model specifications the same. As shown in the figure, the HMM-ILM has the lowest WAIC by a significant amount (more than 5), meaning that it has the best fit to the data. In addition, assuming continuous testing, known infection times, or that no undetected plants were infected, all result in estimating a much flatter distance kernel. For example, for a susceptible plant half a meter away from an infectious plant, our HMM-ILM estimates an infection risk of 39% (23%, 49%), while the model assuming no undetected plants were infected estimates an infection risk of only 19% (12%, 27%), which is half as large. A possible explanation for this difference is that, from Figure 8, many of the undetected plants that were likely infected were adjacent to plants with known infections in the same row, half a meter away. Therefore, if we assume that none of those undetected plants were actually infected, we would expect to see a much smaller estimate of the effect of disease spread between close plants, as we observe in Figure 9 (d). For this example, we would expect to see a large spatial effect, as seen in the HMM-ILM in

Figure 9 (a), as TSWV is transmitted by thrips that move from plant to plant (Mullis et al., 2009).

To help dig deeper into the differences between the models, we give the full set of posterior distributions of each model from Figure 9 in SM Section 5.2. Interestingly, assuming no undetected plants were infected leads to a posterior for  $\theta$  that is concentrated close to one. This makes sense intuitively. If we assume that no undetected plants were infected, then every plant that was infected must have been detected. This then implies a high chance of detecting the disease in a plant. However, since it takes 2-4 weeks for symptoms to appear in a plant (Brust, 2024), it seems unlikely that we would have a probability close to one for a plant to be detected in the same time step it was infected, as implied by this model. Also interestingly, assuming continuous testing leads to a posterior for  $m$  that is concentrated close to one. Again, this makes sense intuitively. If individuals were infectious for more than one time step, then a continuous testing model would heavily imply that we would observe multiple detection times for at least some detected individuals. Therefore, the only way to explain a single detection time for each detected individual is if  $m = 1$ . However, this seems unlikely given plants are infectious with TSWV until death (Cooper and Meadows, 2024).

## 5 Discussion

We have proposed a hidden Markov model for analyzing individual-level outbreak data where we have only a single detection time for each detected individual, which is very common in practice (Stockdale et al., 2017; Kypraios et al., 2017; O'Neill and Kypraios, 2019; Stockdale et al., 2021; Almutiriy et al., 2021). For example, this detection time may correspond to when symptoms first appeared in an individual, as in our examples, or it could represent when individuals first tested positive on a laboratory test (Mizumoto and Chowell, 2020). Unlike most other approaches built around data augmentation methods (O'Neill and Roberts, 1999; O'Neill and Kypraios, 2019), we do not assume the detection times correspond to infection or removal times. As we showed in our examples, important model results, such as estimates of  $R_0$ , can be very sensitive to assumptions about whether the infection or removal times are known. For instance, in our norovirus example, assuming known removal times led to an unrealistically low estimate of between-nurse transmission. In our TSWV example, assuming known infection times resulted in estimating a much flatter distance kernel and a worse model fit. In addition, an often overlooked assumption of the popular known removal times framework of O'Neill and Roberts (1999) is that no infectious individuals can be removed without being detected. This means these models cannot account for infections with mild or no symptoms, when testing is based on the appearance of symptoms, or removals that are

not recorded for other reasons. In contrast, our HMM-ILM allows infectious individuals to recover before testing positive, and we can estimate the number of undetected removals as shown in the norovirus example.

Almutiry et al. (2021) proposed using an SINR model (Jewell et al., 2009) to estimate infection and removal times when both are unknown. However, their framework only estimates the infection and removal times of the detected individuals (e.g., those who showed symptoms) and assumes that none of the undetected individuals were infected. In contrast, our HMM-ILM allows infectious individuals to go undetected if they never test positive. This means, when testing is based on the appearance of symptoms, we can account for undetected individuals who had asymptomatic infections or were just infected late in the study and not yet showing symptoms. For the TSWV example, we found that at least 58 of the undetected plants were likely infected during the experiment, an aspect the analysis of Almutiry et al. (2021) did not account for. In addition, assuming no undetected plants were infected led to estimating a much flatter distance kernel and a worse model fit. Some of the restrictive assumptions in Almutiry et al. (2021) could be relaxed using computationally intensive reversible jump MCMC steps (Jewell et al., 2009). However, these steps only add infection times, not removal times (they assume that removal occurs sometime after the end of the observation period). Therefore, this would only allow for  $S \rightarrow I$  transitions among undetected individuals (e.g, late infections) and not  $S \rightarrow I \rightarrow R$  transitions (e.g, asymptomatic infections), which are allowed by the HMM-ILM.

Touloupou et al. (2020) also analyzed individual-level outbreak data using coupled hidden Markov models. However, they assumed each individual was continuously tested for the disease. If individuals were continuously tested, then we would expect to observe multiple detection times for at least some of the detected individuals. However, in many applications, such as in the examples considered here, we have only a single detection time for each detected individual (Stockdale et al., 2017, 2021; O'Neill and Kypraios, 2019). In the TSWV example, our HMM-ILM fit significantly better than the model of Touloupou et al. (2020) and was able to capture a much stronger spatial effect. If we have only a single detection time for each detected individual, then either individuals stopped being tested after their first positive test, as in the TSWV example (Hughes et al., 1997), or individuals were continuously tested and only the initial detection times were reported by the investigators. Both scenarios should lead to the same observation model (1), as we justify in Section 2.1. Indeed, it seems a necessary condition for modeling such data is that the probability of detection drops to 0 after the first detection, as in Equation (1), or we would expect to observe multiple detection times for at least some of the detected individuals.

We showed that by rewriting Equation (1), we can consider a wide range of observation

processes: testing only up to the first detection (1), continuous testing (12), known removal times (9), and known infection times (11). Future work should consider further observation models. For instance, in the Tristan da Cunha cold example from Becker (1989), they observed the start and end of symptoms for each individual who showed symptoms. This could be modeled by letting  $y_{it}|S_{it} = 2$  follow a Markov chain. We could also consider a multivariate observation vector  $\mathbf{y}_{it}$  in cases where we observe multiple events, such as death and the development of different kinds of symptoms (Neal and Roberts, 2004). In our examples, we found that important results (e.g., estimates of  $R_0$ ) can be very sensitive to assumptions about the observation process, such as whether removal times are known. As such, future work should carefully consider the choice of the observation model based on investigation reports and by using model comparison criteria, such as the WAIC, as we did here.

There are some important limitations of our work. We only consider SIR compartmental models. The iFFBS algorithm, which is the cornerstone of our inferential procedure, only requires that  $S_{it}|\mathbf{S}_{(-i)(t-1)}$  follow a first-order Markov chain (Douwes-Schultz, 2024). Therefore, extensions to more complex compartmental models, such as susceptible-exposed-infectious-removed (SEIR) models (Bu et al., 2025), should be straightforward in theory. However, SEIR models can suffer from serious identifiability problems when only removal times are observed (O'Neill and Kypraios, 2019). The observation process defined in Equation (1) provides less information about the parameters than knowing the removal times (e.g., compare the widths of the posteriors in Figure 5). Therefore, to fit SEIR hidden Markov models, additional data and different observation processes would likely have to be considered, and/or much more informative priors could be used for some of the parameters. A possible solution could be to use the known infection times observation process (11), which, with the additional assumption that there were no undetected infections, is similar to the analysis in Bu et al. (2025) (the justification being that when individuals transition from  $E \rightarrow I$  they show symptoms). However, this would not account for asymptomatic infections. Another limitation is that we assume the test sensitivity,  $\theta$  from Equation (1), is constant. For instance, in the TSWV example, we assume that the probability that an infectious plant develops observable symptoms is the same for every time step it is infected. Since it takes 2-4 weeks for the symptoms to develop, it would be more realistic to let  $\theta$  be 0 for the first time step of infectiousness, an unknown quantity to be estimated for time step 2, and then 0 again after time step 2. That is, if the plant has not developed symptoms after a month or so, it likely will not develop them. This could be accomplished by splitting up the infectious compartment into sub-compartments. Finally, individuals often change their behavior during an epidemic in response to others around them showing symptoms (Ward et al., 2023,

2025) and to their own symptoms. This could be incorporated into the HMM-ILM by letting  $\beta_{j \rightarrow i, t}$  depend on  $y_{i0}, \dots, y_{i(t-1)}$  and  $y_{j0}, \dots, y_{j(t-1)}$ . Note that the iFFBS algorithm allows for autoregression in the transition probabilities (Douwes-Schultz, 2024). We will consider extensions such as this in future work.

## References

Almutiriy, W., KV, V. W. and Deardon, R. (2021) Continuous time individual-level models of infectious disease: Package EpiILMCT. *Journal of Statistical Software*, **98**, 1–44.

Amiri, L., Torabi, M. and Deardon, R. (2024) Spatial modelling of infectious diseases with covariate measurement error. *Journal of the Royal Statistical Society Series C: Applied Statistics*, **73**, 460–477.

Becker, N. G. (1989) *Analysis of Infectious Disease Data*. Chapman and Hall/CRC.

Bilodeau, B., Stringer, A. and Tang, Y. (2024) Stochastic convergence rates and applications of adaptive quadrature in Bayesian inference. *Journal of the American Statistical Association*, **119**, 690–700.

Britton, T. and O'Neill, P. D. (2002) Bayesian inference for stochastic epidemics in populations with random social structure. *Scandinavian Journal of Statistics*, **29**, 375–390.

Brust, G. (2024) The curious case of the virus infected tomato fruit. *Vegetable and Fruit News*, **15**, 3–4.

Bu, F., Aiello, A. E., Volfovsky, A. and Xu, J. (2025) Stochastic EM algorithm for partially observed stochastic epidemics with individual heterogeneity. *Biostatistics*, **26**, kxae018.

Bu, F., Aiello, A. E., Xu, J. and Volfovsky, A. (2022) Likelihood-based inference for partially observed epidemics on dynamic networks. *Journal of the American Statistical Association*, **117**, 510–526.

Cáceres, V. M., Kim, D. K., Bresee, J. S., Horan, J., Noel, J. S., Ando, T., Steed, C. J., Weems, J. J., Monroe, S. S. and Gibson, J. J. (1998) A viral gastroenteritis outbreak associated with person-to-person spread among hospital staff. *Infection Control & Hospital Epidemiology*, **19**, 162–167.

Chib, S. (1996) Calculating posterior distributions and modal estimates in Markov mixture models. *Journal of Econometrics*, **75**, 79–97.

Cohen, S., Doyle, W. J., Skoner, D. P., Rabin, B. S. and Gwaltney, J. M. (1997) Social ties and susceptibility to the common cold. *JAMA*, **277**, 1940–1944.

Cooper, A. and Meadows, I. (2024) Tomato spotted wilt virus on tomato and pepper. Technical report, NC State Extension Publications.

Davies, N. G., Klepac, P., Liu, Y., Prem, K., Jit, M. and Eggo, R. M. (2020) Age-dependent effects in the transmission and control of COVID-19 epidemics. *Nature Medicine*, **26**, 1205–1211.

Deardon, R., Brooks, S. P., Grenfell, B. T., Keeling, M. J., Tildesley, M. J., Savill, N. J., Shaw, D. J. and Woolhouse, M. E. J. (2010) Inference for individual-level models of infectious diseases in large populations. *Statistica Sinica*, **20**, 239.

Douwes-Schultz, D. (2024) *Coupled Markov switching models for spatio-temporal infectious disease counts*. Ph.D. thesis, McGill University. URL: <https://escholarship.mcgill.ca/concern/theses/6395wf20p>.

Douwes-Schultz, D. and Schmidt, A. M. (2022) Zero-state coupled Markov switching count models for spatio-temporal infectious disease spread. *Journal of the Royal Statistical Society: Series C (Applied Statistics)*, **71**, 589–612.

Douwes-Schultz, D., Schmidt, A. M., Shen, Y. and Buckeridge, D. L. (2025) A three-state coupled Markov switching model for COVID-19 outbreaks across Quebec based on hospital admissions. *The Annals of Applied Statistics*, **19**, 371–396.

Frühwirth-Schnatter, S. (2006) *Finite Mixture and Markov Switching Models*. Springer Series in Statistics. New York: Springer-Verlag.

Gelman, A., Hwang, J. and Vehtari, A. (2014) Understanding predictive information criteria for Bayesian models. *Statistics and Computing*, **24**, 997–1016.

Hu, M., Lin, H., Wang, J., Xu, C., Tatem, A. J., Meng, B., Zhang, X., Liu, Y., Wang, P., Wu, G. et al. (2021) Risk of coronavirus disease 2019 transmission in train passengers: an epidemiological and modeling study. *Clinical Infectious Diseases*, **72**, 604–610.

Hughes, G., McRoberts, N., Madden, L. V. and Nelson, S. C. (1997) Validating mathematical models of plant-disease progress in space and time. *Mathematical Medicine and Biology: A Journal of the IMA*, **14**, 85–112.

Jewell, C. P., Kypraios, T., Neal, P. and Roberts, G. O. (2009) Bayesian analysis for emerging infectious diseases. *Bayesian Analysis*, **4**, 465–496.

Keeling, M. J., Woolhouse, M. E., Shaw, D. J., Matthews, L., Chase-Topping, M., Haydon, D. T., Cornell, S. J., Kappey, J., Wilesmith, J. and Grenfell, B. T. (2001) Dynamics of the 2001 UK foot and mouth epidemic: stochastic dispersal in a heterogeneous landscape. *Science*, **294**, 813–817.

Kypraios, T., Neal, P. and Prangle, D. (2017) A tutorial introduction to Bayesian inference for stochastic epidemic models using Approximate Bayesian Computation. *Mathematical Biosciences*, **287**, 42–53.

Lappe, B. L., Wikswo, M. E., Kambhampati, A. K., Mirza, S. A., Tate, J. E., Kraay, A. N. and Lopman, B. A. (2023) Predicting norovirus and rotavirus resurgence in the United States following the COVID-19 pandemic: a mathematical modelling study. *BMC Infectious Diseases*, **23**, 254.

Lekone, P. E. and Finkenstädt, B. F. (2006) Statistical inference in a stochastic epidemic SEIR model with control intervention: Ebola as a case study. *Biometrics*, **62**, 1170–1177.

Lichtemberg, P. S., Moreira, L., Zeviani, W. M., Amorim, L. and De Mio, L. M. (2022) Dispersal gradient of *M. fructicola* conidia from peach orchard to an open field. *European Journal of Plant Pathology*, **162**, 231–236.

Mahsin, M. D., Deardon, R. and Brown, P. (2022) Geographically dependent individual-level models for infectious diseases transmission. *Biostatistics*, **23**, 1–17.

Mizumoto, K. and Chowell, G. (2020) Transmission potential of the novel coronavirus (COVID-19) onboard the diamond Princess Cruises Ship, 2020. *Infectious Disease Modelling*, **5**, 264–270.

Mullis, S. W., Bertrand, P. F., Brown, S. L., Csinos, A. S., Díaz-Pérez, J. C., Gitaitis, R. D., Hickman, L. L., Johnson, A., LaHue, S. S., Martinez, N. et al. (2009) Tospoviruses in Solanaceae and other crops in the coastal plain of Georgia.

Neal, P. J. and Roberts, G. O. (2004) Statistical inference and model selection for the 1861 Hagelloch measles epidemic. *Biostatistics*, **5**, 249–261.

Neal, R. M. (2003) Slice sampling. *The Annals of Statistics*, **31**, 705–767.

Nguyen, M. H., Neyens, T., Lawson, A. B. and Faes, C. (2025) Assessing the impact of neighborhood structures in Bayesian disease mapping. *Journal of Applied Statistics*, 1–17.

O'Neill, P. D. and Roberts, G. O. (1999) Bayesian inference for partially observed stochastic epidemics. *Journal of the Royal Statistical Society. Series A (Statistics in Society)*, **162**, 121–129.

O'Neill, P. D. (2002) A tutorial introduction to Bayesian inference for stochastic epidemic models using Markov chain Monte Carlo methods. *Mathematical Biosciences*, **180**, 103–114.

O'Neill, P. D. and Kypraios, T. (2019) Markov chain Monte Carlo methods for outbreak data. In *Handbook of Infectious Disease Data Analysis*, 159–178. Chapman and Hall/CRC.

Plummer, M., Best, N., Cowles, K. and Vines, K. (2006) CODA: Convergence diagnosis and output analysis for MCMC. *R News*, **6**, 7–11.

Pohle, J., Langrock, R., van der Schaar, M., King, R. and Jensen, F. H. (2021) A primer on coupled state-switching models for multiple interacting time series. *Statistical Modelling*, **21**, 264–285.

Pokharel, G. and Deardon, R. (2014) Supervised learning and prediction of spatial epidemics. *Spatial and Spatio-temporal Epidemiology*, **11**, 59–77.

— (2016) Gaussian process emulators for spatial individual-level models of infectious disease. *Canadian Journal of Statistics*, **44**, 480–501.

— (2022) Emulation-based inference for spatial infectious disease transmission models incorporating event time uncertainty. *Scandinavian Journal of Statistics*, **49**, 455–479.

Reich, B. J. and Ghosh, S. K. (2019) *Bayesian Statistical Methods*. Chapman and Hall/CRC.

Shaby, B. A. and Wells, M. T. (2010) Exploring an adaptive Metropolis algorithm.

Steele, M. K., Wikswo, M. E., Hall, A. J., Koelle, K., Handel, A., Levy, K., Waller, L. A. and Lopman, B. A. (2020) Characterizing norovirus transmission from outbreak data, United States. *Emerging Infectious Diseases*, **26**, 1818.

Stockdale, J. E., Kypraios, T. and O'Neill, P. D. (2017) Modelling and Bayesian analysis of the Abakaliki smallpox data. *Epidemics*, **19**, 13–23.

— (2021) Pair-based likelihood approximations for stochastic epidemic models. *Biostatistics*, **22**, 575–597.

Thompson, D. and Foege, W. (1968) Faith tabernacle smallpox epidemic, Abakaliki, Nigeria. *Report WHO/SE/68.3*, World Health Organization, Geneva, Switzerland. URL: [https://stacks.cdc.gov/view/cdc/21451/cdc\\_21451\\_DS1.pdf](https://stacks.cdc.gov/view/cdc/21451/cdc_21451_DS1.pdf).

Tibbits, M. M., Groendyke, C., Haran, M. and Liechty, J. C. (2014) Automated factor slice sampling. *Journal of Computational and Graphical Statistics*, **23**, 543–563.

Touloupou, P., Finkenstädt, B. and Spencer, S. E. F. (2020) Scalable Bayesian inference for coupled hidden Markov and semi-Markov models. *Journal of Computational and Graphical Statistics*, **29**, 238–249.

de Valpine, P., Turek, D., Paciorek, C. J., Anderson-Bergman, C., Lang, D. T. and Bodik, R. (2017) Programming with models: Writing statistical algorithms for general model structures with NIMBLE. *Journal of Computational and Graphical Statistics*, **26**, 403–413.

Vynnycky, E. and White, R. (2010) *An Introduction to Infectious Disease Modelling*. Oxford University Press.

Wang, J., Gao, Z., Yang, Z.-R., Liu, K. and Zhang, H. (2023) Global prevalence of asymptomatic norovirus infection in outbreaks: a systematic review and meta-analysis. *BMC Infectious Diseases*, **23**, 595.

Ward, C., Deardon, R. and Schmidt, A. M. (2023) Bayesian modeling of dynamic behavioral change during an epidemic. *Infectious Disease Modelling*, **8**, 947–963.

Ward, M. A., Deardon, R. and Deeth, L. E. (2025) A framework for incorporating behavioural change into individual-level spatial epidemic models. *Canadian Journal of Statistics*, **53**, e11828.

Warriyar, V. K., Almutiriy, W. and Deardon, R. (2020) Individual-level modelling of infectious disease data: EpiILM. *The R Journal*, **12**, 87–104.

# Supplementary material for “Hidden Markov Individual-level Models of Infectious Disease Transmission”

Dirk Douwes-Schultz<sup>1\*</sup> , Rob Deardon<sup>1,2</sup> and Alexandra M. Schmidt<sup>3</sup>

<sup>1</sup>*Department of Mathematics and Statistics,*

*University of Calgary, Canada*

<sup>2</sup>*Faculty of Veterinary Medicine,*

*University of Calgary, Canada*

<sup>3</sup>*Department of Epidemiology, Biostatistics and Occupational Health,*

*McGill University, Canada*

February 17, 2026

\*Corresponding author: Dirk Douwes-Schultz, Department of Mathematics and Statistics, University of Calgary, 2500 University Drive NW, Calgary, AB, Canada, T2N 1N4. E-mail: [dirk.douwesschultz@ucalgary.ca](mailto:dirk.douwesschultz@ucalgary.ca).

## Contents

<b>1</b>	<b>The Individual Forward Filtering Backward Sampling (iFFBS) Algorithm</b>	<b>2</b>
<b>2</b>	<b>Simulation Study to Assess Parameter Recovery</b>	<b>5</b>
<b>3</b>	<b>Widely Applicable Information Criterion (WAIC)</b>	<b>12</b>
<b>4</b>	<b>Further Analysis of the Norovirus Example</b>	<b>14</b>
4.1	State estimates . . . . .	14
4.2	Alternative models . . . . .	17
<b>5</b>	<b>Further Analysis of the Tomato Spotted Wilt Virus (TSWV) Example</b>	<b>19</b>
5.1	Alternative distance kernels . . . . .	19
5.2	Posterior distributions . . . . .	23

## 1 The Individual Forward Filtering Backward Sampling (iFFBS) Algorithm

In this section, we will go into more detail concerning the hybrid Gibbs sampling algorithm we use to draw from the joint posterior of  $\mathbf{S}$  and  $\mathbf{v} = (\theta, m, \alpha, \beta)^T$ ,  $p(\mathbf{S}, \mathbf{v} | \mathbf{y})$ . We will borrow all notation from the main text. We first choose initial values for the Gibbs sampler,  $\mathbf{S}^{[0]}$  and  $\mathbf{v}^{[0]}$ . The initial values for the parameter vector  $\mathbf{v}$ ,  $\mathbf{v}^{[0]}$ , are generated randomly within the parameter space. To ensure valid initial values for the state indicators, we first set  $S_{it}^{[0]} = 1$  for all undetected individuals  $i$  and for all  $t$ . Then, for a detected individual  $i$  where  $y_{ik} = 1$ , we let  $S_{it}^{[0]} = 1$  for  $t < k$ ,  $S_{it}^{[0]} = 2$  for  $t = k$ , and  $S_{it}^{[0]} = 3$  for  $t > k$  (if  $y_{ik} = 1$  then  $S_{ik}^{[0]}$  must be 2). If the observation process, Equation (1) in the main text, is changed, then we modify  $\mathbf{S}^{[0]}$  accordingly to ensure  $p(\mathbf{y}, \mathbf{S}^{[0]} | \mathbf{v}^{[0]}) > 0$ ; see Equation (5) of the main text.

After setting the initial values, the following steps are repeated for  $q = 1, \dots, Q$ , where  $Q$  is the total number of iterations for the Gibbs sampler,

1. Sample  $\mathbf{v}^{[q]}$  from  $p(\mathbf{v} | \mathbf{S}^{[q-1]}, \mathbf{y})$ .
2. Sample  $\mathbf{S}_{i(0:T)}^{[q]}$  from  $p(\mathbf{S}_{i(0:T)} | \mathbf{S}_{1(0:T)}^{[q]}, \dots, \mathbf{S}_{i-1(0:T)}^{[q]}, \mathbf{S}_{i+1(0:T)}^{[q-1]}, \dots, \mathbf{S}_{N(0:T)}^{[q-1]}, \mathbf{y}, \mathbf{v}^{[q]})$  for  $i = 1, \dots, N$ .

As mentioned in the main text, step 1 is mainly broken up into slice or Metropolis-Hastings steps. Here, we will provide the iFFBS algorithm needed to sample from  $p(\mathbf{S}_{i(0:T)} | \mathbf{S}_{(-i)(0:T)}, \mathbf{y}, \mathbf{v})$  for step 2. The algorithm was originally proposed by Touloupou et al. (2020). We will sometimes use the subscript  $t_1 : t_2$  to denote a temporally indexed vector subset to the interval  $t_1$  to  $t_2$ , e.g.,  $y_{i(0:t)} = (y_{i0}, \dots, y_{it})^T$ .

First note that,

$$p(\mathbf{S}_{i(0:T)} | \mathbf{S}_{(-i)(0:T)}, \mathbf{y}, \mathbf{v}) = p(S_{iT} | \mathbf{S}_{(-i)(0:T)}, \mathbf{y}, \mathbf{v}) \prod_{t=0}^{T-1} p(S_{it} | S_{i(t+1)}, \mathbf{S}_{(-i)(0:t+1)}, \mathbf{y}_{i(0:t)}, \mathbf{v}). \quad (1)$$

Therefore, to sample  $\mathbf{S}_{i(0:T)}^{[q]}$  from  $p(\mathbf{S}_{i(0:T)} | \mathbf{S}_{(-i)(0:T)}, \mathbf{y}, \mathbf{v})$ , we can sample  $S_{iT}^{[q]}$  from  $p(S_{iT} | \mathbf{S}_{(-i)(0:T)}, \mathbf{y}, \mathbf{v})$ , then  $S_{i(T-1)}^{[q]}$  from  $p(S_{i(T-1)} | S_{iT}^{[q]}, \mathbf{S}_{(-i)(0:T)}, \mathbf{y}_{i(0:T-1)}, \mathbf{v})$ , and so on. Now note that, from Bayes' Theorem,

$$p(S_{it} | S_{i(t+1)}, \mathbf{S}_{(-i)(0:t+1)}, \mathbf{y}_{i(0:t)}, \mathbf{v}) \propto p(S_{i(t+1)} | S_{it}, \mathbf{S}_{(-i)(0:t)}, m, \alpha, \beta) p(S_{it} | \mathbf{S}_{(-i)(0:t+1)}, \mathbf{y}_{i(0:t)}, \mathbf{v}). \quad (2)$$

The first term on the right-hand side of (2),  $p(S_{i(t+1)} | S_{it}, \mathbf{S}_{(-i)(0:t)}, m, \alpha, \beta)$ , can be derived from the transition matrix in Equation (2) of the main text. The probabilities

$P(S_{it} = s | \mathbf{S}_{(-i)(0:t+1)}, \mathbf{y}_{i(0:t)}, \mathbf{v})$  for  $s = 1, 2, 3$  and  $t = 0, \dots, T-1$  and  $P(S_{iT} = s | \mathbf{S}_{(-i)(0:T)}, \mathbf{y}, \mathbf{v})$  for  $s = 1, 2, 3$  are known as the filtered probabilities. These are calculated iteratively using the forward part of the algorithm from  $t = 0$ .

Starting at  $t = 0$  we have,

$$\begin{aligned} p(S_{i0} | \mathbf{S}_{(-i)(0:1)}, y_{i0}, \mathbf{v}) &\propto p(S_{i0}) p(\mathbf{S}_{(-i)1} | \mathbf{S}_{(-i)0}, S_{i0}, m, \alpha, \beta) \\ &\propto p(S_{i0}) \prod_{j: i \in NE(j)} p(S_{j1} | S_{j0}, \mathbf{S}_{(-j)0}, m, \alpha, \beta). \end{aligned} \quad (3)$$

Here,  $p(S_{i0})$  is the initial state distribution, which is set by the modeler, and  $p(S_{j1} | S_{j0}, \mathbf{S}_{(-j)0}, m, \alpha, \beta)$  represents a transition probability of the Markov chain for individual  $j$ . Since  $p(S_{j1} | S_{j0}, \mathbf{S}_{(-j)0}, m, \alpha, \beta)$  only depends on whether individual  $i$  is infectious, only two values of  $\prod_{j: i \in NE(j)} p(S_{j1} | S_{j0}, \mathbf{S}_{(-j)0}, m, \alpha, \beta)$  need to be calculated. Also, since  $S_{i0}$  can only take three values, it is straightforward to derive the filtered probabilities from (3),

$$P(S_{i0} = s | \mathbf{S}_{(-i)(0:1)}, y_{i0}, \mathbf{v}) = \frac{P(S_{i0} = s) \prod_{\substack{j: i \in NE(j) \\ S_{i0}=s}} p(S_{j1} | S_{j0}, \mathbf{S}_{(-j)0}, m, \alpha, \beta)}{\sum_{k=1}^3 P(S_{i0} = k) \prod_{\substack{j: i \in NE(j) \\ S_{i0}=k}} p(S_{j1} | S_{j0}, \mathbf{S}_{(-j)0}, m, \alpha, \beta)}, \quad (4)$$

for  $s = 1, 2, 3$ .

For  $t = 1, \dots, T-1$ , we have

$$\begin{aligned} p(S_{it} | \mathbf{S}_{(-i)(0:t+1)}, \mathbf{y}_{i(0:t)}, \mathbf{v}) &\propto p(y_{it} | S_{it}, \mathbf{y}_{i(0:t-1)}, \theta) p(S_{it} | \mathbf{S}_{(-i)(0:t)}, \mathbf{y}_{i(0:t-1)}, \mathbf{v}) \\ &\quad \times \prod_{j:i \in NE(j)} p(S_{j(t+1)} | S_{jt}, \mathbf{S}_{(-j)t}, m, \alpha, \boldsymbol{\beta}). \end{aligned}$$

Here,  $p(y_{it} | S_{it}, \mathbf{y}_{i(0:t-1)}, \theta)$  is given by the observation model from Equation (1) in the main text. The probabilities  $P(S_{it} = s | \mathbf{S}_{(-i)(0:t)}, \mathbf{y}_{i(0:t-1)}, \mathbf{v})$  for  $s = 1, 2, 3$  are known as the predictive probabilities and can be calculated as follows,

$$\begin{aligned} P(S_{it} = s | \mathbf{S}_{(-i)(0:t)}, \mathbf{y}_{i(0:t-1)}, \mathbf{v}) &= \\ \sum_{k=1}^3 P(S_{it} = s | S_{i(t-1)} = k, \mathbf{S}_{(-i)(t-1)}, m, \alpha, \boldsymbol{\beta}) P(S_{i(t-1)} = k | \mathbf{S}_{(-i)(0:t)}, \mathbf{y}_{i(0:t-1)}, \mathbf{v}), \end{aligned}$$

where  $P(S_{i(t-1)} = k | \mathbf{S}_{(-i)(0:t)}, \mathbf{y}_{i(0:t-1)}, \mathbf{v})$  for  $k = 1, 2, 3$  are the previous filtered probabilities.

It then follows that,

$$\begin{aligned} P(S_{it} = s | \mathbf{S}_{(-i)(0:t+1)}, \mathbf{y}_{i(0:t)}, \mathbf{v}) &= \\ p(y_{it} | S_{it} = s, \mathbf{y}_{i(0:t-1)}, \theta) P(S_{it} = s | \mathbf{S}_{(-i)(0:t)}, \mathbf{y}_{i(0:t-1)}, \mathbf{v}) &\quad \prod_{\substack{j:i \in NE(j) \\ S_{it}=s}} p(S_{j(t+1)} | S_{jt}, \mathbf{S}_{(-j)t}, m, \alpha, \boldsymbol{\beta}) \\ \overline{\sum_{k=1}^3 p(y_{it} | S_{it} = k, \mathbf{y}_{i(0:t-1)}, \theta) P(S_{it} = k | \mathbf{S}_{(-i)(0:t)}, \mathbf{y}_{i(0:t-1)}, \mathbf{v})} &\quad \prod_{\substack{j:i \in NE(j) \\ S_{it}=k}} p(S_{j(t+1)} | S_{jt}, \mathbf{S}_{(-j)t}, m, \alpha, \boldsymbol{\beta}) \end{aligned} \tag{5}$$

for  $s = 1, 2, 3$ .

Calculating the filtered probabilities for  $t = T$  is similar except there are no forward product terms,

$$P(S_{iT} = s | \mathbf{S}_{(-i)(0:T)}, \mathbf{y}, \mathbf{v}) = \frac{p(y_{iT} | S_{iT} = s, \mathbf{y}_{i(0:T-1)}, \theta) P(S_{iT} = s | \mathbf{S}_{(-i)(0:T)}, \mathbf{y}_{i(0:T-1)}, \mathbf{v})}{\sum_{k=1}^3 p(y_{iT} | S_{iT} = k, \mathbf{y}_{i(0:T-1)}, \theta) P(S_{iT} = k | \mathbf{S}_{(-i)(0:T)}, \mathbf{y}_{i(0:T-1)}, \mathbf{v})}, \tag{6}$$

for  $s = 1, 2, 3$ .

Once the filtered probabilities have been calculated  $\mathbf{S}_{i(0:T)}$  can be sampled backwards using Equations (1) and (2). Firstly,  $S_{iT}^{[q]}$  is sampled from  $p(S_{iT} | \mathbf{S}_{(-i)(0:T)}, \mathbf{y}, \mathbf{v})$  using (6). Then, for  $t = T - 1, \dots, 0$ ,  $S_{it}^{[q]}$  is drawn from the density defined by,

$$P(S_{it} = s | S_{i(t+1)} = S_{i(t+1)}^{[q]}, \mathbf{S}_{(-i)(0:t+1)}, \mathbf{y}_{i(0:t)}, \mathbf{v}) = \frac{P(S_{i(t+1)} = S_{i(t+1)}^{[q]} | S_{it} = s, \mathbf{S}_{(-i)t}, m, \alpha, \beta) P(S_{it} = s | \mathbf{S}_{(-i)(0:t+1)}, \mathbf{y}_{i(0:t)}, \mathbf{v})}{\sum_{k=1}^3 P(S_{i(t+1)} = S_{i(t+1)}^{[q]} | S_{it} = k, \mathbf{S}_{(-i)t}, m, \alpha, \beta) P(S_{it} = k | \mathbf{S}_{(-i)(0:t+1)}, \mathbf{y}_{i(0:t)}, \mathbf{v})},$$

for  $s = 1, 2, 3$ . Here,  $P(S_{it} = s | \mathbf{S}_{(-i)(0:t+1)}, \mathbf{y}_{i(0:t)}, \mathbf{v})$  is given by either Equation (5) or (4) (for  $t=0$ ).

In NIMBLE, we code the iFFBS algorithm on the log scale to improve numerical stability. All NIMBLE R code for the custom iFFBS samplers is provided on GitHub ([https://github.com/Dirk-Douwes-Schultz/HMM\\_ILM\\_Code](https://github.com/Dirk-Douwes-Schultz/HMM_ILM_Code)). Note that the only calculations that separate the iFFBS algorithm from a traditional FFBS algorithm for hidden Markov models (Chib, 1996; Frühwirth-Schnatter, 2006) are the forward product terms  $\prod_{j:i \in NE(j)} p(S_{j(t+1)} | S_{jt}, \mathbf{S}_{(-j)t}, m, \alpha, \beta)$ , which are needed to account for between chain dependencies.

## 2 Simulation Study to Assess Parameter Recovery

We designed a simulation study to ensure that our hybrid Gibbs sampling algorithm could recover the true parameter values of the HMM-ILM. We simulated repeatedly from an HMM-ILM specified as in the tomato spotted wilt virus (TSWV) example in Section 4.2 of the main text. As in that example, we assumed  $N = 520$  individuals in a 26-by-20 grid, with a meter between rows and half a meter between individuals within the same row (see Figure 6 in the main text). We assumed that the individuals were observed over  $t = 1, \dots, T = 7$  time periods and that at  $t = 0$ , each individual had a 1% chance of being initially infected. We

specified the effect of disease spread from individual  $j$  to individual  $i$ , see Equations (2)-(3) in the main text, as

$$\beta_{j \rightarrow i, t} = \beta_{j \rightarrow i} = \beta_0 d_{ij}^{-a} (1 - \ln(d_{ij})(\beta_1 - a) + 0.5 \ln(d_{ij})^2 (\beta_1 - a)^2),$$

where  $d_{ij}$  is the distance between the two individuals and  $a = 1.35$ . Finally, we let  $NE(i)$ , from Equation (3) of the main text, include all individuals at most three individuals away from individual  $i$ , including on the diagonal. See Section 4.2 of the main text for more details on how the above specifications were determined.

For the true parameter values, we took the posterior medians estimated in Section 4.2 of the main text:  $\theta = 0.55$ ,  $m = 16$ ,  $\alpha = 0.015$ ,  $\beta_0 = 0.07$ , and  $\beta_1 = 3$ . The values for  $\theta$  and  $m$  mean that if an individual becomes infected, they have a 55% chance of being detected at each time step and that the infectious period lasts an average of 16 time steps. The values for  $\alpha$ ,  $\beta_0$ , and  $\beta_1$  yield a fairly short range of dispersal for the disease; see Figure 7 in the main text. We simulated from the above HMM-ILM 232 times (originally we ran 250 simulations; however, 18 did not finish within their allotted time, which is normal for the computing cluster we use). Figure 1 below shows one of the simulated outbreaks.

We fit a correctly specified HMM-ILM to each of the 232 simulated outbreaks using our hybrid Gibbs sampling algorithm. We used the same independent prior distributions as in Section 4.2 of the main text:  $m \sim \text{Unif}(1, 20)$ ,  $\theta \sim \text{Unif}(0, 1)$ ,  $\alpha \sim \text{Unif}(0, 1)$ ,  $\beta_0 \sim \text{Unif}(0, 1)$ , and  $\beta_1 \sim \text{Unif}(0, 20)$ . As in the main text, we ran our hybrid Gibbs sampling algorithm for 200,000 iterations on three chains with an initial burn-in of 50,000 iterations. We placed an automated factor slice sampler (Tibbits et al., 2014) on the entire parameter vector  $\mathbf{v} = (m, \theta, \alpha, \beta_0, \beta_1)^T$ . Since we cannot visually assess the convergence for all 232 fits, we wanted to ensure the best possible mixing for  $\mathbf{v}$ . For each fit, convergence was checked using the minimum effective sample size ( $> 1000$ ) and the maximum Gelman-Rubin statistic ( $< 1.05$ ) (Plummer et al., 2006). Our Gibbs sampler passed the convergence checks for

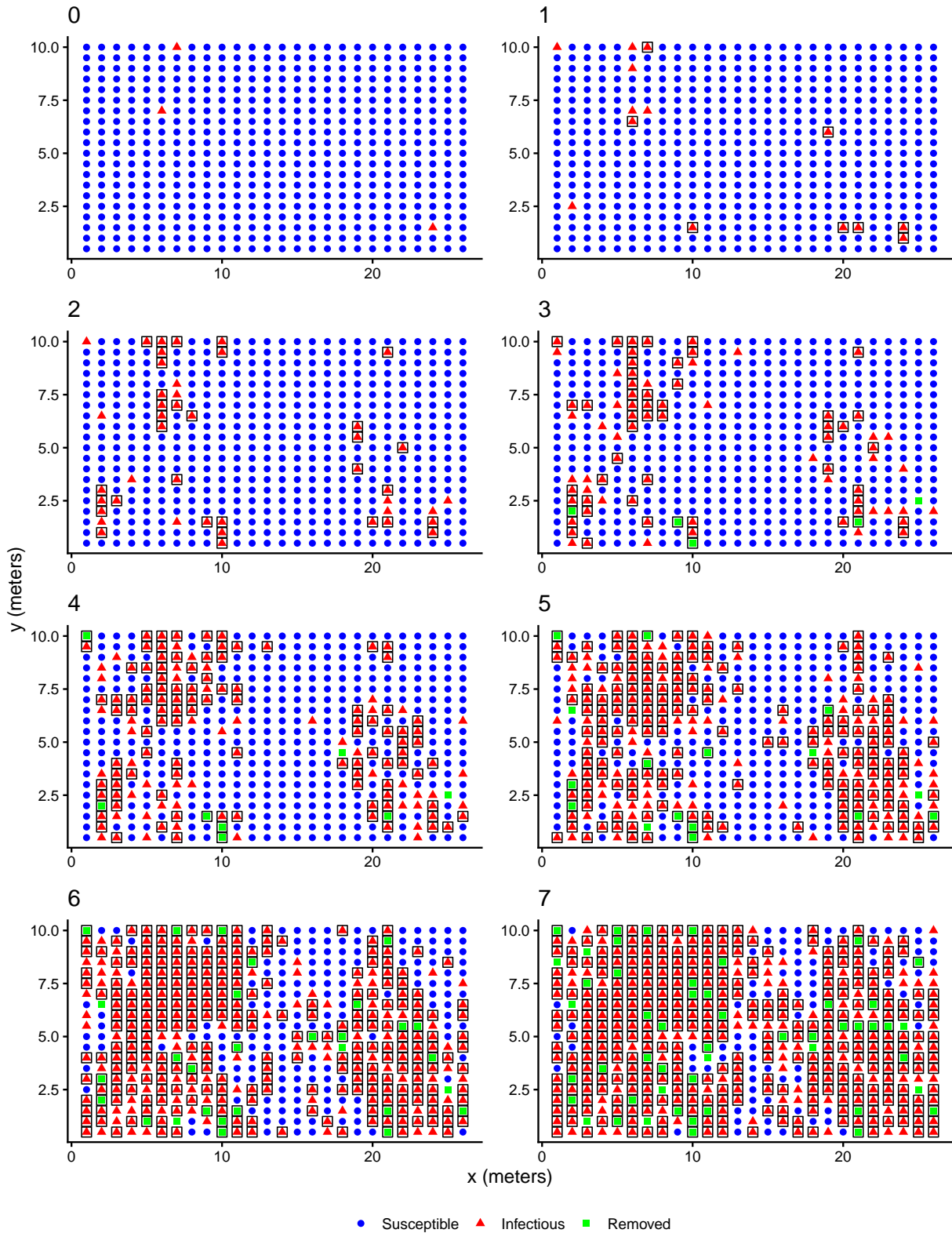


**Figure 1:** Shows one of the simulated outbreaks from the simulation study in SM Section 2 with  $m = 16$ . A box is drawn around individuals who have been detected. From the final plot, there are 83 undetected infections in total (i.e., 83 red triangles or green squares without boxes around them).

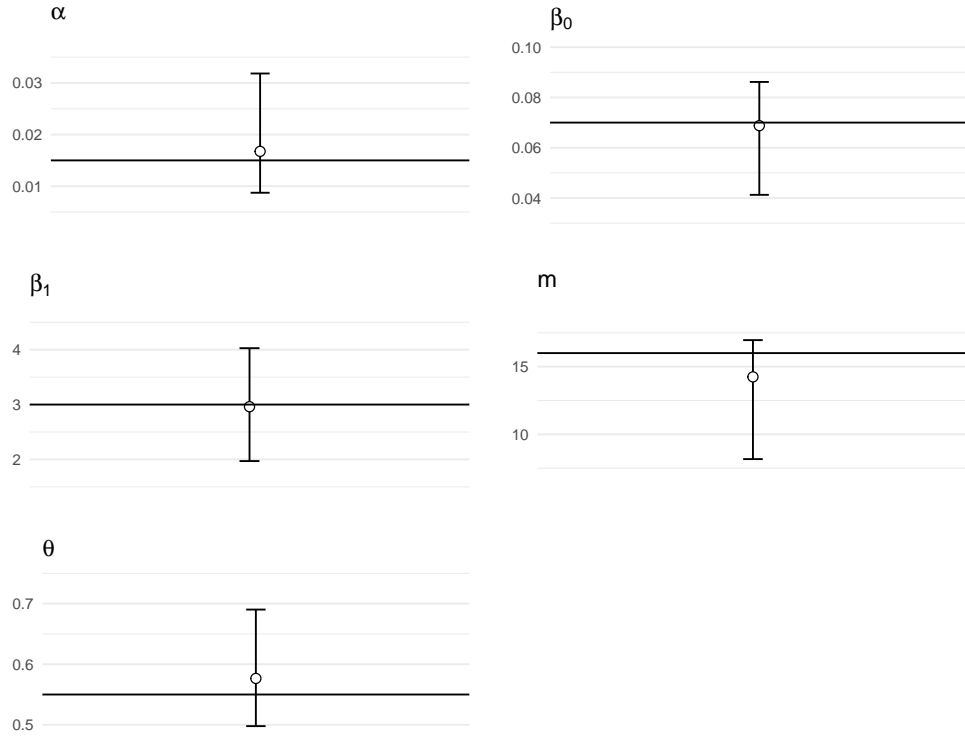


**Figure 2:** Shows the sample medians (circles) and 95% quantile intervals (.025 and .975 quantiles) (caps) of the posterior medians from fitting 230 replications of the HMM-ILM described in SM Section 2 with  $m=16$ . The horizontal lines are drawn at the true parameter values.

$230/232 = 99.14\%$  of the simulations, illustrating a good convergence rate.

Figure 2 shows the sample medians and 95% quantile intervals (0.025 and 0.975 quantiles) of the 230 posterior medians from the converged fits. The horizontal lines are drawn at the true parameter values. From the figure, the posteriors of  $\alpha$ ,  $\beta_0$ , and  $\beta_1$  are all centered very close to the true parameter values on average. The posteriors of  $\theta$  and  $m$  are centered slightly off the true parameter values on average (the sample medians of the 230 posterior medians are .58 and 14.24 versus true values of .55 and 16, respectively). However, the discrepancy is not large enough to dramatically change any conclusions and seems to result from relatively flat marginal posterior distributions; the left-hand graph of Figure 3 shows the posterior distribution of  $m$  from fitting one of the simulations.

Due to the flatness in the posterior, the left-hand plot of Figure 3 suggests it may be

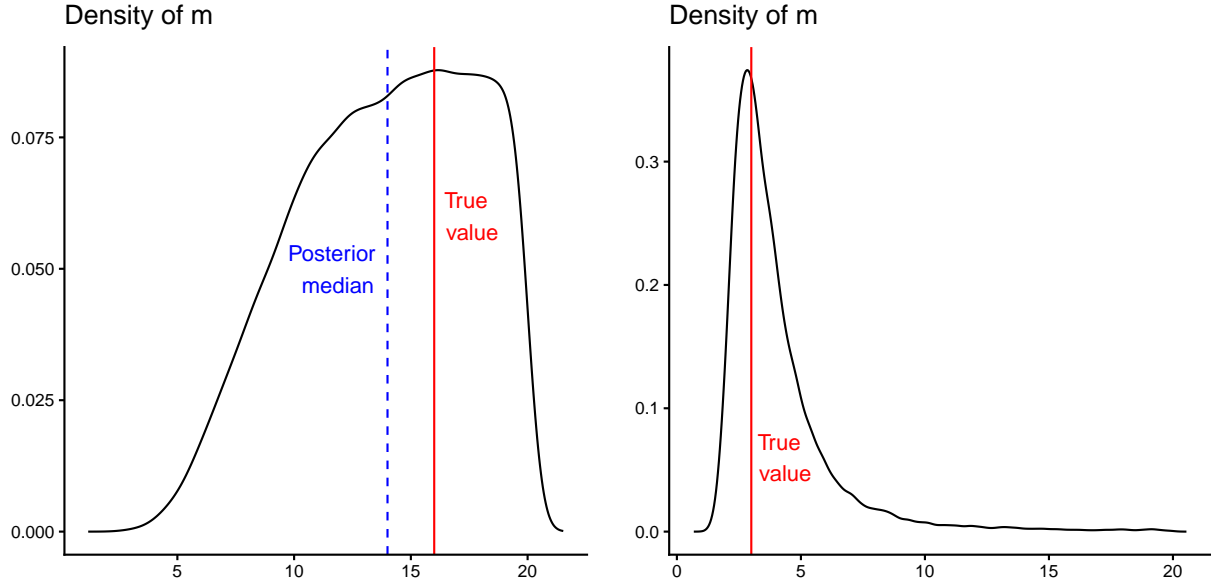


**Figure 3:** Shows the posterior distribution of  $m$  from fitting a single simulation of the HMM-ILM described in SM Section 2 with  $m = 16$  (left) and  $m = 3$  (right).

difficult to estimate  $m$  when the true value is greater than  $T$ , the length of the observation period. We also observed this flatness in the posterior of  $m$  for the TSWV example in Section 4.2 of the main text. For sensitivity analysis, we ran/fit an additional simulation with  $m = 3$  instead of 16. The posterior distribution of  $m$  for this additional simulation is given in the right-hand plot of Figure 3. From the plot, the posterior of  $m$  is much more concentrated around the true parameter value when the true value is less than  $T$  compared to when the true value is greater than  $T$ .

Table 1 shows the coverage and average width of the 95% credible intervals. The average coverage of the 95% credible intervals is 95.91%, which is close to the nominal values. However, the coverage of  $m$  is relatively high at 99.56%. This is likely due to the truncation of the prior distribution,  $m \sim \text{Unif}(1, 20)$ . For sensitivity analysis, we refit each of the 230 replications using an unbounded prior for  $m$ ,  $1/m \sim \text{Unif}(0, 1)$  (or  $p(m) = m^{-2}I[m > 1]$ ). Our Gibbs sampler converged for all but 2 of the 230 simulations when using the new prior. The results for  $\alpha$ ,  $\beta_0$ ,  $\beta_1$ , and  $\theta$  were all very similar to those shown in Table 1 and Figure 2, so we will not report them here. The coverage of the 95% credible interval for  $m$  went from 99.56%

**Table 1:** Shows the coverage and average width of the 95% credible intervals (CIs) from the simulation study in SM Section 2 with  $m = 16$  and prior  $m \sim \text{Unif}(1, 20)$ .

Parameter	Coverage of 95% CI (%)	Average Width of 95% CI
$\alpha$	93.91	0.02
$\beta_0$	95.22	0.04
$\beta_1$	95.65	2.00
$m$	99.56	13.03
$\theta$	95.21	0.23

to 96.26%. However, the average width of the credible interval went from 13.03 to 211.55. Indeed, the 95% credible interval for  $m$  often included values as high as 80 years or so, which is not realistic as the length of the infectious period. Therefore, some upper bound on  $m$  seems necessary, and we recommend using a  $\text{Unif}(0, b)$  prior as we do in the main text. Note, having the prior for  $m$  quickly approach 0 does not appear to be enough to prevent the large width of the credible interval, since  $p(m) = m^{-2}I[m > 1]$  does rapidly converge to 0.

Finally, to help visualize the individual simulation results, Figure 4 shows the posterior medians and 95% credible intervals from fitting the first 10 replications. Interestingly, there is considerable variation in the widths of the credible intervals across simulations. This shows that even with the same underlying true parameter values, different outbreaks can carry vastly different amounts of information about the parameters.

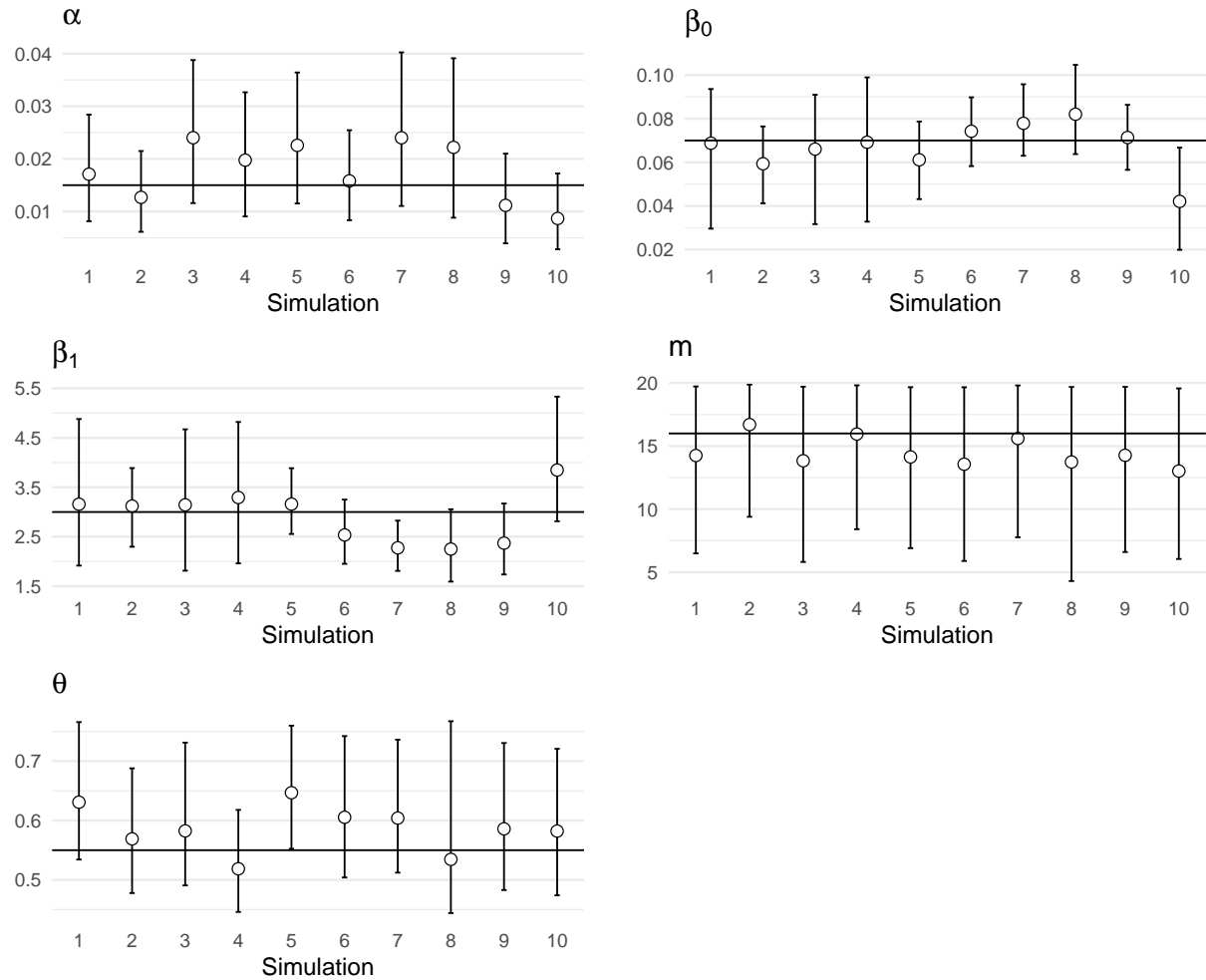


**Figure 4:** Shows the posterior medians (circles) and 95% credible intervals (caps) from fitting the first 10 replications of the HMM-ILM described in SM Section 2 with  $m=16$  and prior  $m \sim \text{Unif}(1, 20)$ . The horizontal lines are drawn at the true parameter values.

### 3 Widely Applicable Information Criterion (WAIC)

The widely applicable information criterion (WAIC) is a popular model selection criterion for Bayesian models (Gelman et al., 2014; Reich and Ghosh, 2019). However, it is not immediately clear how to calculate the WAIC for a state-space model due to the complex dependency structure of such models (Auger-Méthé et al., 2021). One possibility is to calculate the WAIC conditional on the underlying latent states (Auger-Méthé et al., 2021; Kreuzer et al., 2022), which for the HMM-ILM is equivalent to,

$$\begin{aligned} \text{lpdd}^{\text{cond}} &= \sum_{i=1}^N \sum_{t=1}^T \log \left( \frac{1}{Q-M} \sum_{q=M+1}^Q p(y_{it} | S_{it}^{[q]}, y_{i0}, \dots, y_{i(t-1)}, \theta^{[q]}) \right), \\ \text{pwaic}^{\text{cond}} &= \sum_{i=1}^N \sum_{t=1}^T \text{Var}_{q=M+1}^Q \log \left( p(y_{it} | S_{it}^{[q]}, y_{i0}, \dots, y_{i(t-1)}, \theta^{[q]}) \right), \\ \text{WAIC}^{\text{cond}} &= -2(\text{lpdd}^{\text{cond}} - \text{pwaic}^{\text{cond}}), \end{aligned} \quad (7)$$

where the superscript  $[q]$  denotes a draw from the posterior distribution of the variable,  $Q$  is the total number of MCMC samples,  $M$  is the size of the burn-in sample, and  $\text{Var}$  denotes the sample variance. However, as discussed by Auger-Méthé et al. (2021), the conditional WAIC often fails to select the true model, and they recommend marginalizing out the latent states when calculating the WAIC. For the HMM-ILM, this is equivalent to,

$$\begin{aligned} \text{lpdd}^{\text{marg}} &= \sum_{t=1}^T \log \left( \frac{1}{Q-M} \sum_{q=M+1}^Q p(\mathbf{y}_t | \mathbf{y}_0, \dots, \mathbf{y}_{t-1}, \mathbf{v}^{[q]}) \right), \\ \text{pwaic}^{\text{marg}} &= \sum_{t=1}^T \text{Var}_{q=M+1}^Q \log \left( p(\mathbf{y}_t | \mathbf{y}_0, \dots, \mathbf{y}_{t-1}, \mathbf{v}^{[q]}) \right), \\ \text{WAIC}^{\text{marg}} &= -2(\text{lpdd}^{\text{marg}} - \text{pwaic}^{\text{marg}}). \end{aligned} \quad (8)$$

However, calculating  $p(\mathbf{y}_t | \mathbf{y}_0, \dots, \mathbf{y}_{t-1}, \mathbf{v})$  requires running Hamilton's forward filter (Frühwirth-Schnatter, 2006), which requires matrix multiplication with  $\Gamma(\mathbf{S}_t)$ , a  $3^N$  by  $3^N$  matrix. Therefore, it is not computationally feasible to calculate (8).

To deal with the above issues, we follow Douwes-Schultz et al. (2025) and use a partially marginalized version of the WAIC. The idea is to marginalize as much of  $\mathbf{S}$  as possible out of  $p(y_{it}|S_{it}, y_{i0}, \dots, y_{i(t-1)}, \theta) = p(y_{it}|\mathbf{S}, y_{i0}, \dots, y_{i(t-1)}, \theta)$  in Equation (7). Note that from Equation (5) above, we can run the forward part of the iFFBS algorithm to calculate,

$$p(y_{it}|\mathbf{S}_{(-i)(0:t)}, y_{i0}, \dots, y_{i(t-1)}, \mathbf{v}) = \sum_{k=1}^3 p(y_{it}|S_{it} = k, \mathbf{y}_{i(0:t-1)}, \theta) P(S_{it} = k|\mathbf{S}_{(-i)(0:t)}, \mathbf{y}_{i(0:t-1)}, \mathbf{v}). \quad (9)$$

That is, we can marginalize all the states for individual  $i$  and all future states for the other individuals. Therefore, to calculate the WAIC, we use  $p(y_{it}|\mathbf{S}_{(-i)(0:t)}^{[q]}, y_{i0}, \dots, y_{i(t-1)}, \mathbf{v}^{[q]})$  in place of  $p(y_{it}|S_{it}^{[q]}, y_{i0}, \dots, y_{i(t-1)}, \theta^{[q]})$  in Equation (7). It was shown in Douwes-Schultz et al. (2025), through a simulation study, that the WAIC calculated in this manner can distinguish between different coupled hidden Markov models.

Note that  $p(y_{it}|\mathbf{S}_{(-i)(0:t)}, y_{i0}, \dots, y_{i(t-1)}, \mathbf{v})$  in Equation (9) has a convenient interpretation. It represents the distribution of  $y_{it}$  given knowledge of the disease states of all other individuals through time  $t$ . Therefore, models that are effective at borrowing information between individuals will have lower WAICs, which would seem to be a desirable property for an epidemic model.

## 4 Further Analysis of the Norovirus Example

### 4.1 State estimates

The posterior probability that nurse  $i$  was susceptible ( $s = 1$ ), infectious ( $s = 2$ ), or removed ( $s = 3$ ) on day  $t$  can be approximated by  $P(S_{it} = s|\mathbf{y}) \approx \frac{1}{Q-M} \sum_{q=M+1}^Q I[S_{it}^{[q]} = s]$  for  $i = 1, \dots, 89$  and  $t = 0, \dots, 9$ . By viewing plots of  $P(S_{it} = s|\mathbf{y})$  versus  $t$  for various nurses, we can better understand how the outbreak evolved over time. For example, Figure 5 shows the state estimates for Nurse X (Nurse 1) and Nurse 2 (one of the four nurses detected on the seventh). From the figure, we can see that Nurse X was likely infectious at the beginning of the outbreak (i.e., was the index case) and not removed until at least the seventh or eighth. Nurse 2 was likely infected on the fifth or sixth and not removed until at least the ninth or tenth. Examining plots of the other detected nurses showed a similar pattern of at least 2-4 days from detection to removal and 1-2 days between infection and detection.

It is also interesting to view plots of  $P(S_{it} = s|\mathbf{y})$  versus  $t$  for the undetected nurses. Figure 6 shows the state estimates for Nurse 29, who is the first undetected nurse. Note that, due to the homogeneous mixing assumption, the undetected nurses are indistinguishable, so the state estimates for any other undetected nurse would be the same as in Figure 6. From the figure, we can see that there is a 25% chance that an undetected nurse was in the infectious or removed state at the end of the observation period. This implies there should have been around  $0.25 * 61 \approx 15$  undetected infections. We can more formally estimate the number of undetected infections by looking at the posterior median and 95% credible interval of  $\sum_{i=29}^{89} I[S_{iT} = 2 \text{ or } 3]$ , which is 14 (4, 35). Therefore, there is quite a lot of uncertainty around the exact number of undetected infections that occurred.

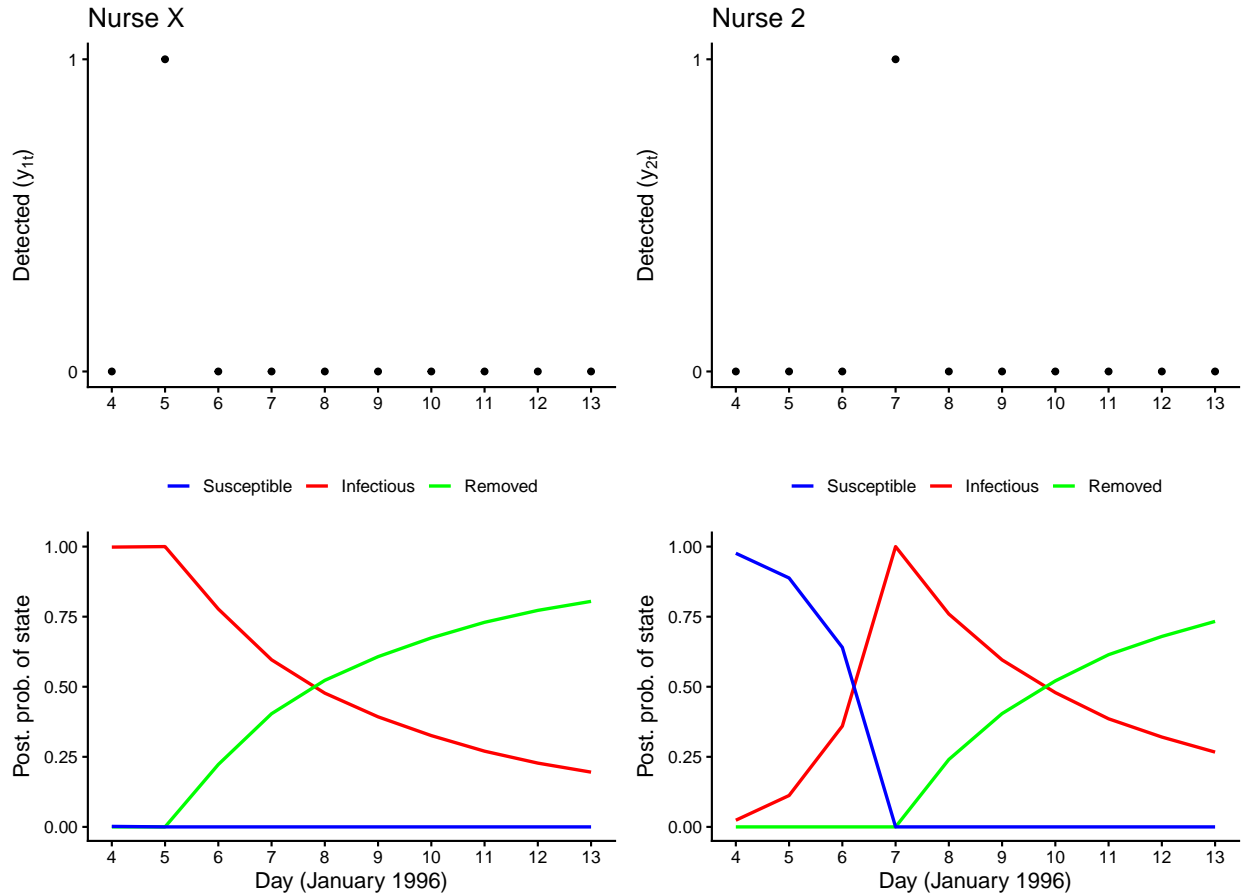


**Figure 5:** The top graphs show the day the nurse was detected (i.e., first reported showing symptoms). The bottom graphs show the posterior probability that the nurse was in the susceptible (blue), infectious (red), and removed (green) states during each day. Nurse X refers to the first nurse detected on the fifth. Nurse 2 refers to one of the four nurses detected on the seventh.

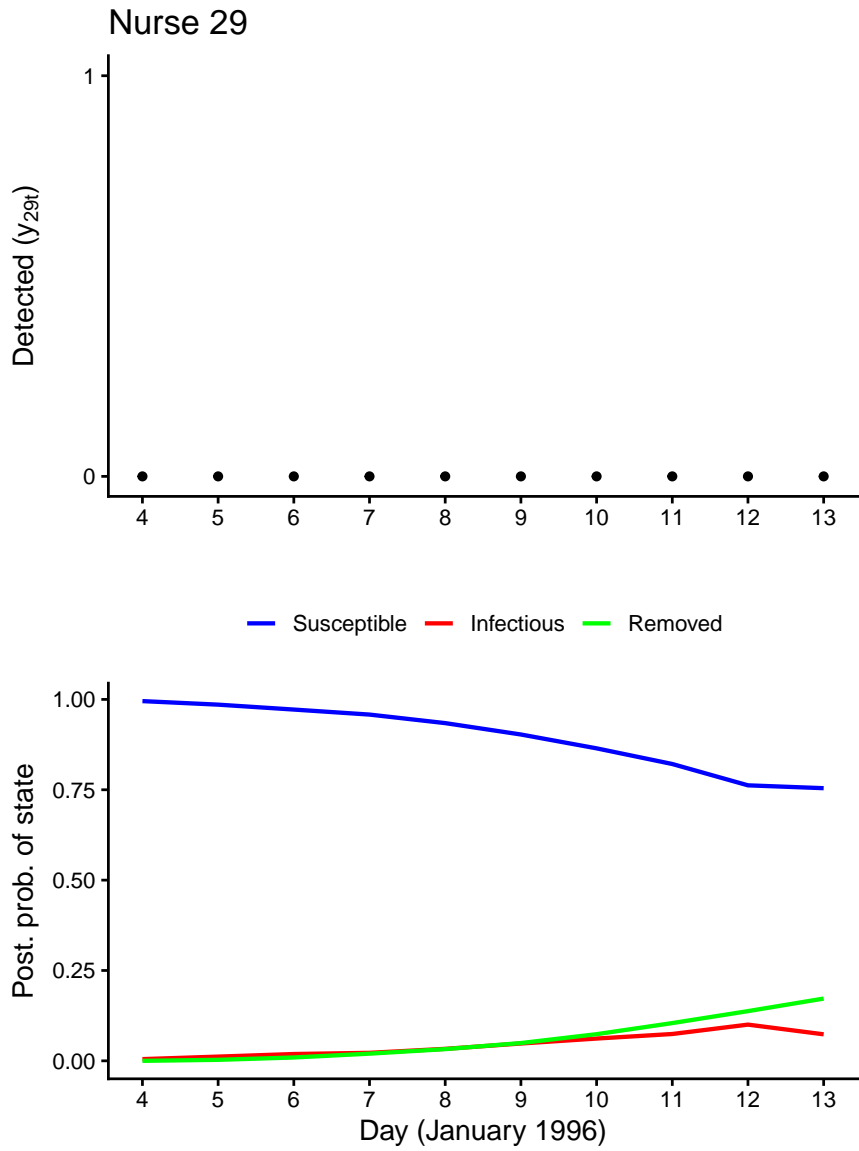


**Figure 6:** The top graphs show the day the nurse was detected (i.e., first reported showing symptoms). The bottom graphs show the posterior probability that the nurse was in the susceptible (blue), infectious (red), and removed (green) states during each day. Nurse 29 refers to the first undetected nurse.

## 4.2 Alternative models

When analyzing the norovirus outbreak described in Section 4.1 of the main text, Kypraios et al. (2017) made the following assumptions:

- (i) That all removal times in the interval  $[1, T]$  had been observed and were equal to the detection times (i.e, the reported symptom onset times).
- (ii) That there were no undetected infections.
- (iii) That the ward was always open.
- (iv) That there was no background infection risk. That is, they did not include an intercept in their model.

Assumption (i) appears to be the most commonly made in the literature when analyzing incomplete individual-level epidemic data (O'Neill and Roberts, 1999; O'Neill and Kypraios, 2019). Therefore, in the main text, we focused on investigating the impact of Assumption (i), represented by the known removal times (KRT) model, compared with assuming the removal times had not been observed, represented by the HMM-ILM. Here, we will additionally investigate the consequences of Assumptions (ii)-(iv).

Assumption (ii) is also common (Britton and O'Neill, 2002; Almutiray et al., 2021) as, traditionally, it avoids the use of complex reversible jump MCMC steps (O'Neill and Roberts, 1999; Jewell et al., 2009). We can incorporate Assumption (ii) by fixing  $S_{it} = 1$  for all undetected nurses  $i = 29, \dots, 89$  and  $t = 0, \dots, 9$ . We can incorporate Assumption (iii) by setting  $W_t = 0$  for all  $t = 0, \dots, 9$  in Equation (8) of the main text. Finally, we can incorporate assumption (iv) by fixing  $\alpha = 0$  in Equation (3) of the main text. This means that nurses can only be infected by other nurses; that is, there are no background sources of infection.

Table 2 compares the WAIC and posterior summaries of  $R_0$  between the HMM-ILM from the main text (which, recall, does not assume the removal times are known), an HMM-ILM with Assumption (i) (the KRT model from the main text), an HMM-ILM with Assumptions (i)+(iii), an HMM-ILM with Assumptions (i)+(iii)+(ii), and an HMM-ILM with Assumptions

**Table 2:** Shows the WAIC and the posterior median and 95% CI of  $R_0$  for five models fitted to the norovirus outbreak. See Section 4.1 of the main text and Section 4.2 for a description of the models.

Model	$R_0$ (posterior median and 95% CI)	WAIC
Unknown removal times (HMM-ILM from main text)	2.61 (1, 7.04)	221
Known removal times (KRT model from main text)	0.65 (0.04, 1.82)	222.36
Known removal times + Ward always open	0.64 (0.04, 1.81)	222.35
Known removal times + Ward always open + No undetected infections	0.73 (0.11, 1.52)	222.28
Known removal times + Ward always open + No undetected infections + No intercept	1.26 (0.81, 1.92)	222.61

(i)+(iii)+(ii)+(iv). For any model including Assumption (i), we used the same priors as the KRT model from the main text,  $m \sim \text{Unif}(1, 3)$ ,  $\alpha \sim \text{Unif}(0, 1)$  (if  $\alpha$  was included), and  $\beta \sim \text{Unif}(0, 1)$ . In addition, as explained in the main text, for any model including Assumption (i), we replaced Equation (1) from the main text with Equation (9) from the main text.

As shown in the table, all models have similar WAIC values despite some models' estimates of  $R_0$  being very different. This suggests that there is not enough information in the only 28 detection times to distinguish between different epidemic model structures using model comparison criteria. We discuss this issue in more detail in the main text.

From Table 2, the only assumptions that have a large impact on the results are whether the removal times have been observed and whether an intercept is included. We compare the HMM-ILM and KRT models in detail in the main text. Whether to include an intercept

depends on whether a nurse could have been infected only by another nurse or whether there were background sources of infection. We would argue for including the intercept, since there were 10 infected patients on the ward during the observation period who could have infected the nurses (Cáceres et al., 1998). As shown in the table, excluding the intercept increases the estimates of  $R_0$ . This makes sense intuitively. The basic reproduction number measures the amount of infection risk due to between-nurse mixing. If there are no background sources of infection (i.e., no intercept), then all infection risk has to come from between-nurse mixing.

## 5 Further Analysis of the Tomato Spotted Wilt Virus (TSWV) Example

### 5.1 Alternative distance kernels

Here, we compare the following distance kernels for fitting the HMM-ILM to the TSWV experiment in Section 4.2 of the main text:

- (a) Power-law Taylor:  $\beta_{j \rightarrow i} = \beta_0 d_{ij}^{-a} (1 - \ln(d_{ij})(\beta_1 - a) + 0.5 \ln(d_{ij})^2(\beta_1 - a)^2)$ , where  $a=1.35$  (used in the main text).
- (b) Power-law exact:  $\beta_{j \rightarrow i} = \beta_0 \beta_1^{-d_{ij}}$ .
- (c) Neighborhood order:  $\beta_{j \rightarrow i} = \beta_0 I[j \in NE_1(i)] + \beta_1 I[j \in NE_2(i)] + \beta_2 I[j \in NE_3(i)]$ , where  $NE_k(i)$  denotes the set of all  $k$ th order neighbors assuming a queen neighborhood structure (Nguyen et al., 2025) and, therefore,  $NE(i) = NE_1(i) \cup NE_2(i) \cup NE_3(i)$ .
- (d) Linear:  $\beta_{j \rightarrow i} = \beta_0 + \beta_1(3.36 - d_{ij})$ , where 3.36 meters is the maximum distance between plants  $i$  and  $j \in NE(i)$ .
- (e) Quadratic:  $\beta_{j \rightarrow i} = \beta_0 + \beta_1(3.36 - d_{ij}) + \beta_2(3.36 - d_{ij})^2$ , constrained to be positive (see below).
- (f) Spline:  $\beta_{j \rightarrow i} = \beta_0 \eta_0(d_{ij}) + \beta_1 \eta_1(d_{ij}) + \beta_2 \eta_2(d_{ij})$ , where  $\eta_k(d_{ij})$  are basis functions (see below).

For comparing the kernels, we used the same neighborhood set  $NE(i)$  as in the main text

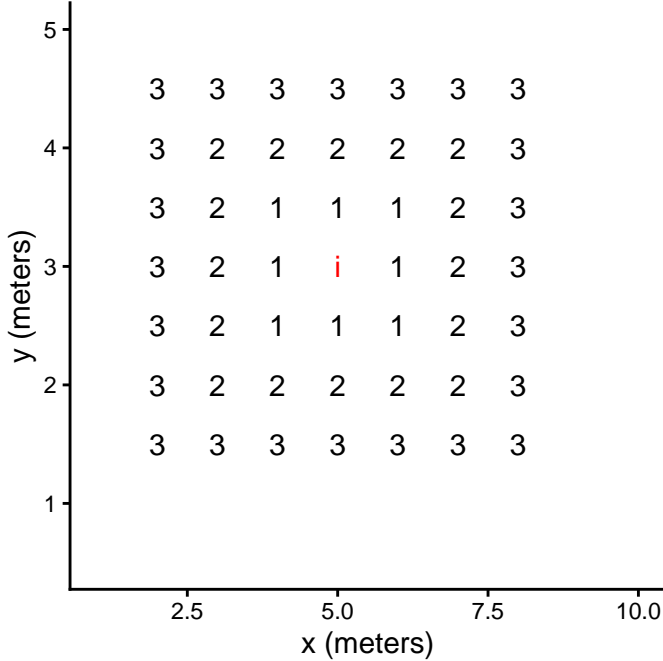


**Figure 7:** Shows the first, second, and third order neighbors of plant  $i$ . Note that the neighborhood set  $NE(i)$  used in the main text consists of all first, second, and third-order neighbors (that is, all the plants numbered on the grid).

and the same priors for  $\alpha$  and  $\theta$ . By the  $k$ th-order neighbors  $NE_k(i)$ , we mean as in Nguyen et al. (2025), assuming a queen neighborhood structure; see Figure 7. The neighborhood set  $NE(i)$  used in the main text is equal to  $NE_1(i) \cup NE_2(i) \cup NE_3(i)$  and, as can be seen in Figure 7, consists of all plants at most 3 plants away from plant  $i$ , including moving diagonally. For the neighborhood order kernel,  $\beta_0$  represents the effect of disease spread from first-order neighbors,  $\beta_1$  represents the effect of disease spread from second-order neighbors, and  $\beta_2$  represents the effect of disease spread from third-order neighbors. We used wide priors for these effects,  $\beta_k \sim \text{Unif}(0, 1)$  for  $k = 0, 1, 2$ .

For the linear kernel, we also used a wide prior for  $\beta_k \sim \text{Unif}(0, 1)$  for  $k = 0, 1$ . To ensure the quadratic kernel is positive on the interval  $[0.5, 3.36]$  (0.5 meters is the minimum distance between plants), we imposed the constraints  $\beta_0 > 0$ ,  $\beta_1 > 0$ , and  $-\beta_1 - 2\beta_2(3.36 - .5) < 0$ . These constraints also force the kernel to be strictly decreasing on  $[0.5, 3.36]$ , which is sensible, as we would expect plants farther away to have a lower effect of disease spread. We used

**Table 3:** Shows the WAIC from fitting the HMM-ILM to the TSWV experiment with six different distance kernels. See Section 5.1 for a description of the kernels.

Kernel	WAIC
Power-law Taylor	1591.76
Power-law exact	1592.24
Neighborhood order	1619.14
Linear	1619.93
Quadratic	1613.29
Spline	1608.22

a wide prior for  $\beta_0 \sim \text{Unif}(0, 1)$  (the effect of disease spread from plants 3.36 meters away),  $\beta_1 \sim \text{Unif}(0, 20)$ , and  $\beta_2 \sim N(0, \sigma = 5)$ .

For the spline kernel, we used nonnegative natural cubic basis functions constructed using the splines2 package (Wang and Yan, 2021). We placed a single internal knot at 1.8 meters, which is the average distance between plants  $i$  and  $j \in NE(i)$ . An issue with the spline kernel is that the number of free parameters equals the number of internal knots plus 2. Therefore, using the spline kernel requires estimating a large number of parameters, which is difficult given the amount of missing information in the data. We decided to add only a single internal knot, since the number of free parameters is already at 3, which is one greater than the power-law kernels. We used a wide prior for  $\beta_k \sim \text{Unif}(0, 5)$  for  $k = 0, 1, 2$ .

Table 3 compares the WAIC of the six distance kernels. The power-law Taylor kernel has the lowest WAIC, indicating it has the best fit to the data. The difference in WAIC between the power-law Taylor kernel and the non-power-law kernels is significant (greater than 5). The power-law exact kernel has a WAIC very similar to that of the power-law Taylor kernel. This makes sense, as the power-law Taylor kernel is a second-order Taylor approximation of the power-law exact kernel. It also shows that the Taylor approximation does not have a negative effect on the fit of the model. Note that many of the differences in WAIC in Table 3 are greater than 5, meaning that we can distinguish fairly well between different distance

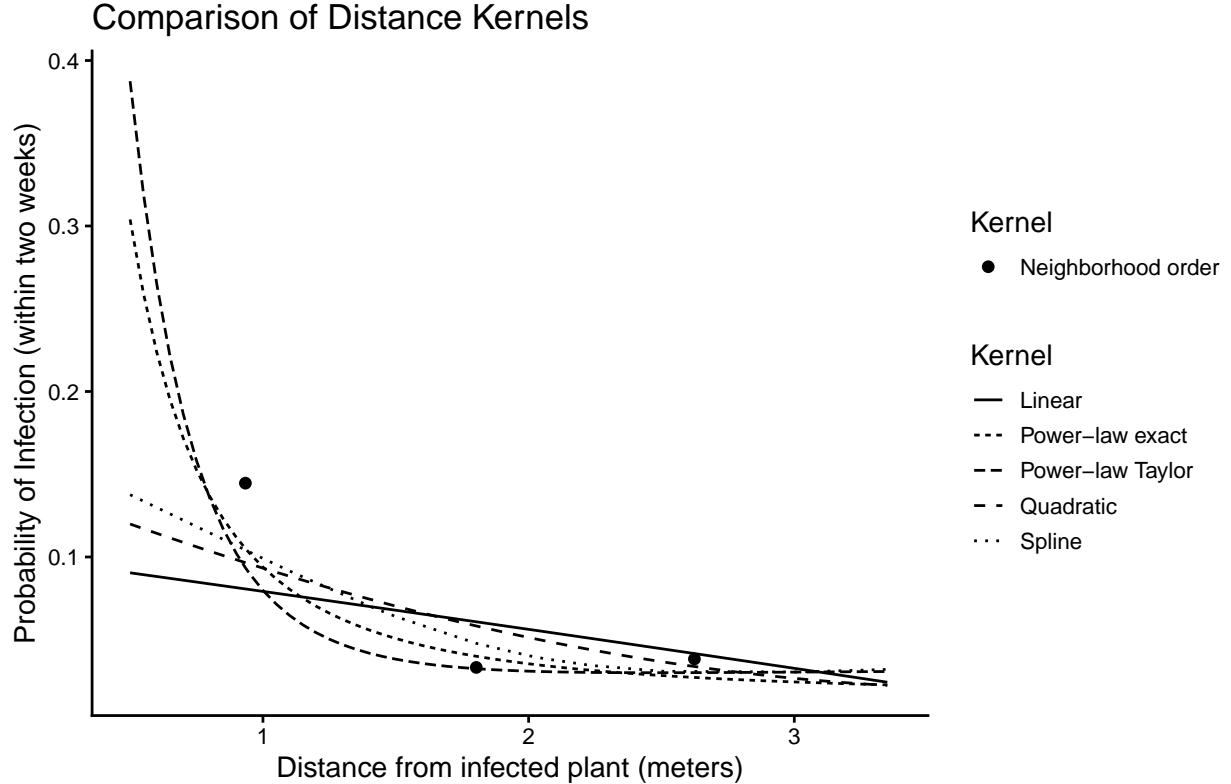


**Figure 8:** Shows the probability that a susceptible plant is infected (within two weeks), given a single infectious plant as a function of the distance between the two plants, for six distance kernels. Shows the posterior medians. Note that the neighborhood order kernel is not a function of distance but of neighborhood order (1,2,3). Therefore, we placed the points at the average distance between plants  $i$  and  $j \in NE_k(i)$  for  $k = 1, 2, 3$ .

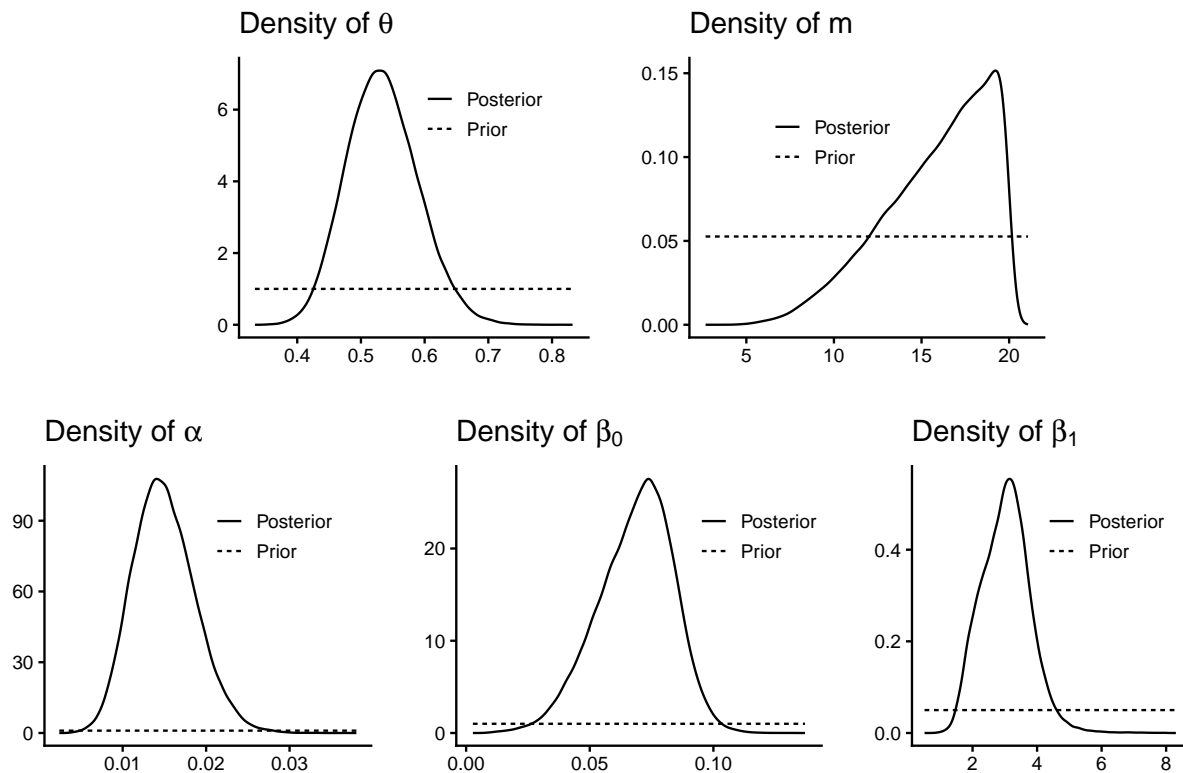
kernels using WAIC at this sample size (327 detection times). In particular, moving from the linear kernel to the quadratic kernel, then to the spline kernel, and finally to the power-law kernels, all show a significant decrease in WAIC.

Figure 8 shows the probability of infection for a susceptible plant versus distance from an infectious plant for the six distance kernels. The power-law kernels estimate a much higher risk of infection for a susceptible plant that is half a meter away (one above or below in the same row) from an infectious plant. However, all kernels agree that there is little infection risk beyond 3 meters, indicating that the disease has a short range of dispersal. Overall, the figure shows that the kernels eventually converge, but that estimates of the effect of disease spread between close plants can be very sensitive to the choice of kernel.

## 5.2 Posterior distributions

Here, we present the complete set of posterior distributions for the models shown in Figure 9 of the main text. Figure 9 shows the posteriors for the HMM-ILM, Figure 10 shows the posteriors for the Touloupou (2020) model, Figure 11 shows the posteriors for the model assuming known infection times, and Figure 12 shows the posteriors of the model assuming no undetected plants were infected. See Section 4.2 of the main text for a description of each model.

### HMM-ILM



**Figure 9:** Shows the posterior and prior distributions of  $\theta$ ,  $m$ ,  $\alpha$ ,  $\beta_0$ , and  $\beta_1$  from fitting the HMM-ILM from Section 4.2 of the main text to the TSWV experiment.

Touloupou (2020)

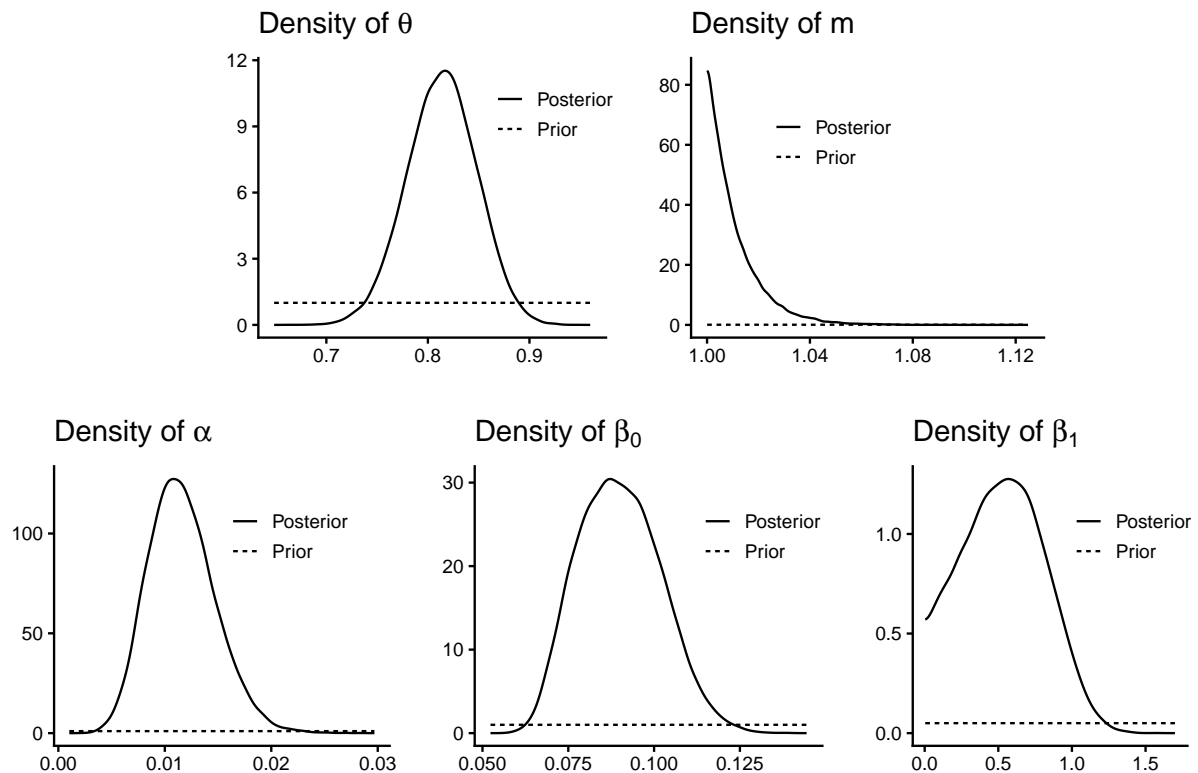


**Figure 10:** Shows the posterior and prior distributions of  $\theta$ ,  $m$ ,  $\alpha$ ,  $\beta_0$ , and  $\beta_1$  from fitting the Touloupou (2020) model from Section 4.2 of the main text to the TSWV experiment.

## Known infection times

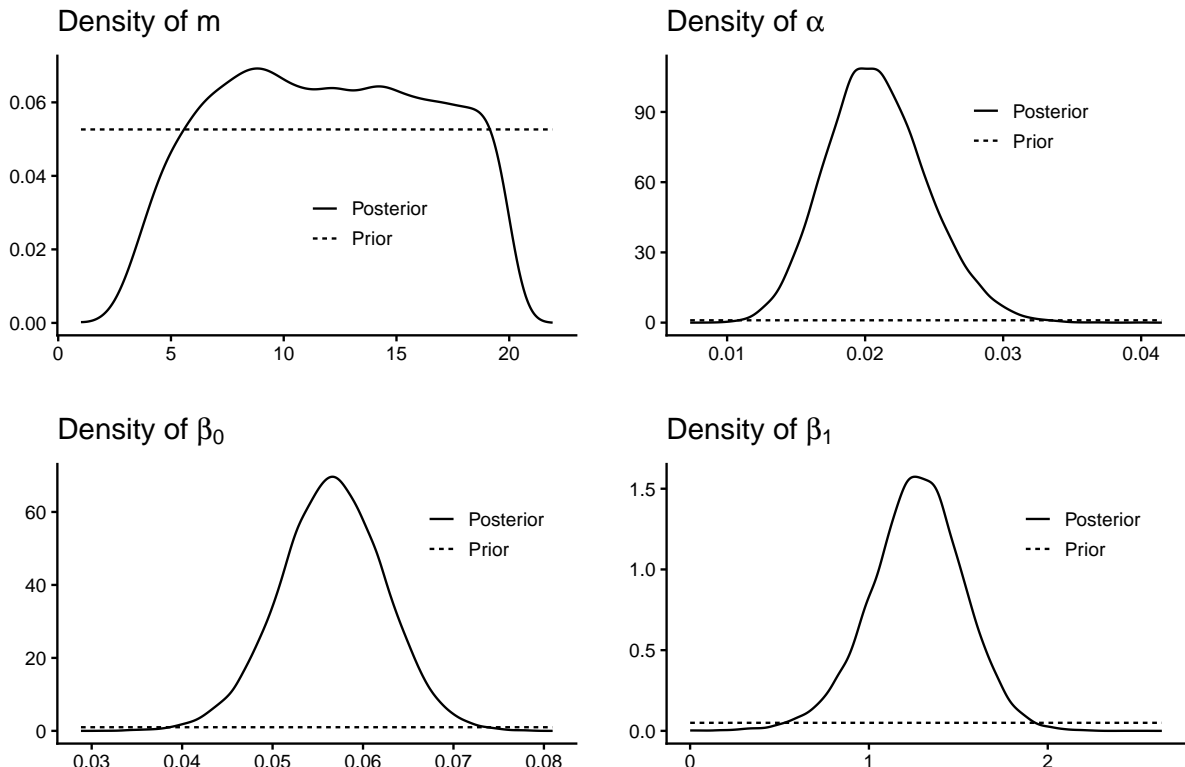


**Figure 11:** Shows the posterior and prior distributions of  $m$ ,  $\alpha$ ,  $\beta_0$ , and  $\beta_1$  from fitting the model assuming known infection times from Section 4.2 of the main text to the TSWV experiment.

No undetected plants infected

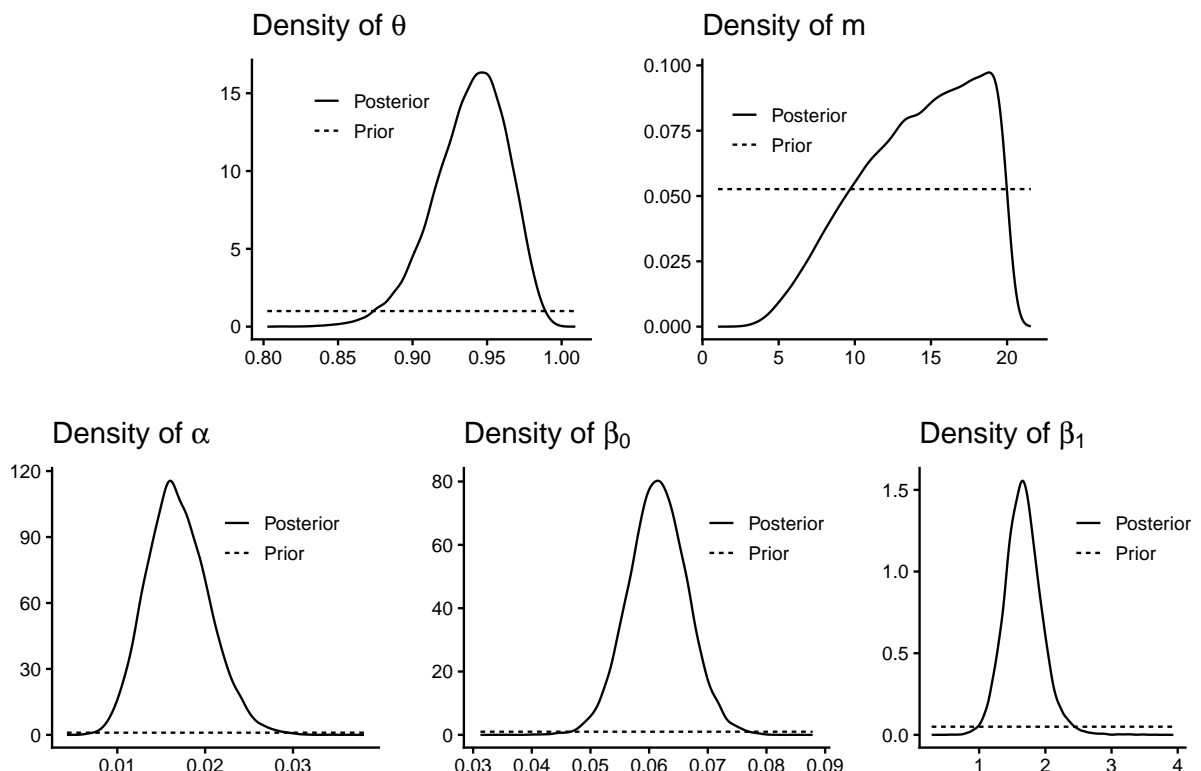


**Figure 12:** Shows the posterior and prior distributions of  $\theta$ ,  $m$ ,  $\alpha$ ,  $\beta_0$ , and  $\beta_1$  from fitting the model assuming no undetected plants were infected from Section 4.2 of the main text to the TSWV experiment.

## References

Almutiry, W., KV, V. W. and Deardon, R. (2021) Continuous time individual-level models of infectious disease: Package EpiILMCT. *Journal of Statistical Software*, **98**, 1–44.

Auger-Méthé, M., Newman, K., Cole, D., Empacher, F., Gryba, R., King, A. A., Leos-Barajas, V., Mills Flemming, J., Nielsen, A., Petris, G. and Thomas, L. (2021) A guide to state-space modeling of ecological time series. *Ecological Monographs*, **91**, e01470.

Britton, T. and O'Neill, P. D. (2002) Bayesian inference for stochastic epidemics in populations with random social structure. *Scandinavian Journal of Statistics*, **29**, 375–390.

Cáceres, V. M., Kim, D. K., Bresee, J. S., Horan, J., Noel, J. S., Ando, T., Steed, C. J., Weems, J. J., Monroe, S. S. and Gibson, J. J. (1998) A viral gastroenteritis outbreak associated with person-to-person spread among hospital staff. *Infection Control & Hospital Epidemiology*, **19**, 162–167.

Chib, S. (1996) Calculating posterior distributions and modal estimates in Markov mixture models. *Journal of Econometrics*, **75**, 79–97.

Douwes-Schultz, D., Schmidt, A. M., Shen, Y. and Buckeridge, D. L. (2025) A three-state coupled Markov switching model for COVID-19 outbreaks across Quebec based on hospital admissions. *The Annals of Applied Statistics*, **19**, 371–396.

Frühwirth-Schnatter, S. (2006) *Finite Mixture and Markov Switching Models*. Springer Series in Statistics. New York: Springer-Verlag.

Gelman, A., Hwang, J. and Vehtari, A. (2014) Understanding predictive information criteria for Bayesian models. *Statistics and Computing*, **24**, 997–1016.

Jewell, C. P., Kypraios, T., Neal, P. and Roberts, G. O. (2009) Bayesian analysis for emerging infectious diseases. *Bayesian Analysis*, **4**, 465–496.

Kreuzer, A., Dalla Valle, L. and Czado, C. (2022) A Bayesian non-linear state space copula model for air pollution in Beijing. *Journal of the Royal Statistical Society Series C: Applied Statistics*, **71**, 613–638.

Kypraios, T., Neal, P. and Prangle, D. (2017) A tutorial introduction to Bayesian inference for stochastic epidemic models using Approximate Bayesian Computation. *Mathematical Biosciences*, **287**, 42–53.

Nguyen, M. H., Neyens, T., Lawson, A. B. and Faes, C. (2025) Assessing the impact of neighborhood structures in Bayesian disease mapping. *Journal of Applied Statistics*, 1–17.

O'Neill, P. D. and Roberts, G. O. (1999) Bayesian inference for partially observed stochastic epidemics. *Journal of the Royal Statistical Society. Series A (Statistics in Society)*, **162**, 121–129.

O'Neill, P. D. and Kypraios, T. (2019) Markov chain Monte Carlo methods for outbreak data. In *Handbook of Infectious Disease Data Analysis*, 159–178. Chapman and Hall/CRC.

Plummer, M., Best, N., Cowles, K. and Vines, K. (2006) CODA: Convergence diagnosis and output analysis for MCMC. *R News*, **6**, 7–11.

Reich, B. J. and Ghosh, S. K. (2019) *Bayesian Statistical Methods*. Chapman and Hall/CRC.

Tibbits, M. M., Groendyke, C., Haran, M. and Liechty, J. C. (2014) Automated factor slice sampling. *Journal of Computational and Graphical Statistics*, **23**, 543–563.

Touloupou, P., Finkenstädt, B. and Spencer, S. E. F. (2020) Scalable Bayesian inference for coupled hidden Markov and semi-Markov models. *Journal of Computational and Graphical Statistics*, **29**, 238–249.

Wang, W. and Yan, J. (2021) Shape-restricted regression splines with R package splines2. *Journal of Data Science*, **19**, 498–517.